Design of a Carbon Dioxide Compression Train

For high pressures and low mass flows, using rolling piston compressors

P.J.N. Bergstein

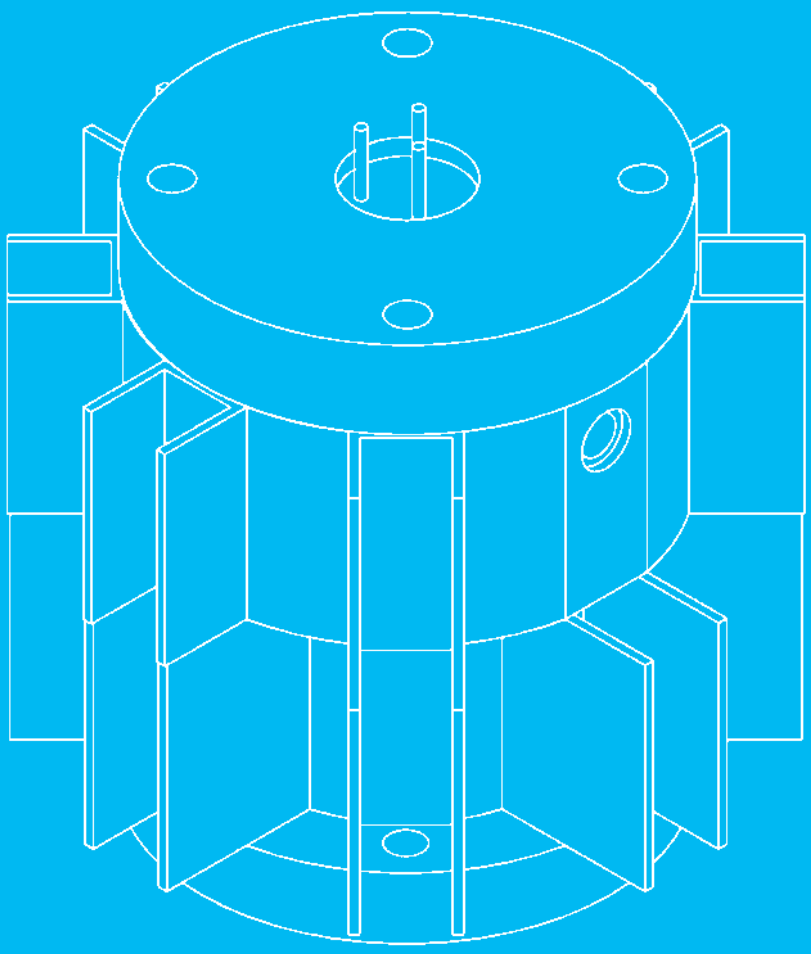

Technische Universiteit Delft

TU Delft

DESIGN OF A CARBON DIOXIDE COMPRESSION TRAIN

FOR HIGH PRESSURES AND LOW MASS FLOWS, USING ROLLING PISTON COMPRESSORS

by

P.J.N. Bergstein

to obtain the degree of Master of Science
at the Delft University of Technology,
to be defended publicly on Friday July 9, 2021 at 10:30 AM.

Student number:	4380142	
Project duration:	Oktober 13, 2020 – July 9, 2021	
Thesis committee:	Prof. dr. ir. B.J. Boersma,	TU Delft, supervisor
	Dr. R. Delfos,	TU Delft
	Dr.ir J.W.R. Peeters,	TU Delft
	Ir. J. van Kranendonk,	Zero Emission Fuels, daily supervisor

This thesis is confidential and cannot be made public until July 8, 2023.

TU Delft Delft University of Technology

ABSTRACT

To answer the need for renewable fuels, Zero Emission Fuels is designing a microplant to create methanol from carbon dioxide and water from the ambient air using only renewable energy from solar panels. For this microplant, gaseous carbon dioxide must be compressed from 1 to 50 [bar] with the low mass flow of 336.7 [g/h]. This thesis examines the compression system which uses rolling piston compressors. This thesis also examines a solution to compress the carbon dioxide optimally.

Because of the low mass flows, the compressors are very small and have relatively high friction and leakage losses. Meanwhile, due to the high pressure ratio of the system, the temperature increase due to compression also poses a problem for the lubrication of the system. Therefore, this thesis looks for solutions for these problems while trying to gain a better understanding of what exactly is happening inside the compressors.

For the temperature regulation, different options for active cooling were assessed with a dimensionless analysis. Eventually, the concept of cooling through the compressor housing was chosen. Afterwards, a computational model was made to calculate the inner workings of the compressors and assess whether the concept of active cooling would still work. Then the computational model was verified by doing experimentation.

After that, the results from the model and the experimentation were compared. The model was able to predict the mass flow and the outside heat transfer coefficient accurately. However, the model was still off from the experimental values by quite a margin. After assessing all the data, the system seemed to perform better as a 2-stage system then as a 3-stage system. However, due to the inaccuracies of the model and experimentation, a definite recommendation on the number of stages of the system cannot be formed.

ACKNOWLEDGEMENTS

I have been working on the compression system of Zero Emission Fuels for almost a year now and found it very interesting to apply all the technical knowledge I have gained over the years at the TU Delft into this project. However, these results could not have been achieved without the help of Jan, Ulrich, Mrigank, Hessel, Samir, Jim, Don, Oumaima, Ilias, Thorsten, Rui, Sander and all the other people at ZEF. I would also like to thank my supervisor Bendiks Jan Boersma who gave my helpful advise and helped me stay on the right track to finish my thesis.

Met deze thesis sluit ik ook een goed gevulde studententijd af waarin ik mij ontplooid heb en ontzettend veel plezier beleefd heb. Daarvoor zou ik graag willen bedanken: mijn jaarclub JC Onyx waar ik hopelijk de rest van mijn leven zoet mee zal zijn en nog veel leuke reizen en borrels mee zal beleven; de oud- en huidige bewoners van 5 angry men waarmee ik altijd heerlijke avonden vol discussies en infantiel vermaak had en zal blijven hebben; mijn hockeyteam Dopie Vief; Virgiel wintersport commissie Paapschnee; de heren van HeerenVerticale Zebra en mijn commissies binnen Gezelschap Leeghwater.

Daarnaast zou ik graag mijn vader en moeder willen bedanken omdat zij er altijd voor mij zijn geweest en mij altijd zijn blijven ondersteunen. Ik zou graag mijn broer en zusje willen bedanken. Dankzij hen heb ik een 2de thuis kunnen vormen in Delft, dat ver weg ligt van ons ouderlijk huis in Bunde. Tot slot zou ik Rivka willen bedanken voor al haar steun, gezelligheid, liefde en prachtige momenten die wij tot nu toe samen hebben gehad.

Pieter Bergstein,

Rotterdam, June 2021

CONTENTS

NOMENCLATURE

Abbreviations

2D	Two Dimensional
3D	Three Dimensional
AC	Alternating Current
AEC	Alkaline Electrolytic Cell
Bi	Biot Number
DAC	Direct Air Capture
DC	Direct Current
FM	Fluid Machinery
MS	Methanol Synthesis
NTC	Negative Temperature Coefficient
Nu	Nusselt Number
Oh	Ohnesorge Number
Pr	Prandtl Number
RPM	Revolutions Per Minute
Ta	Taylor Number
We	Weber Number
ZEF	Zero emission fuels

Constants

π	Ratio of a circle's circumference to its diameter	3.141592653589793
R	Gas constant	8.31446261815324 [J/molK]

Greek symbols

β	Fin parameter
γ	Ratio of specific heats

η	Efficiency	
θ	Angle	[rad]
μ	Dynamic viscosity	[Pa/s]
ν	Kinematic viscosity	$[m^2/s]$
ρ	Density	$[kg/m^3]$
σ	Surface tension	[N/m]
Υ	Ratio between roller and cylinder radii	
ω	Angular velocity	[rad/s]

Molecular Structures

CO_2	Carbon dioxide
H_2	Hydrogen
H_2O	Water
MeOH	Methanol
PFA	Perfluoroalkoxy alkane
POE	Polyolester

Roman symbols

A	Surface area	$[m^2]$
C_p	Specific heat at constant pressure	[J/kgK]
C_v	Specific heat at constant volume	[J/kgK]
D	Diameter	[m]
f	Dimensionless factor	
H	Enthalpy	[J/kg]
h	Heat transfer coefficient	$[W/m^2K]$
k	Thermal conductiviy	[W/mK]
L	Length	[m]
M	Molecular weight	[kg/mol]
m	Mass	[kg]
$\dot{m}$	Mass flow	[kg/s]

n	Amount of substance	[mol]
P	Circumference	[m]
p	Pressure	[Pa]
Q	Heat	[W]
R_x	Thermal resistance	[K/W]
r	Radius	[m]
S	Entropy	[J/K]
T	Temperature	[K]
t	Thickness	$[m^3]$
t	Time	[s]
u	Velocity	[m/s]
V	Volume	$[m^3]$
v	Specific volume	$[m^3/kg]$
W	Work	[W]
x	Location along the fin	[m]

Subscripts

1	Inlet conditions or start of step or inner length
2	Conditions after valve throughput calculations
2	Outlet conditions or end of step or outer length
air	Conditions of air
alu	Conditions of aluminium
avg	Average
b	Base of the fin
c	Compressor chamber
cap	Top and bottom cap combined
he	height of the channel
w	Width of the channel
CO_2	Conditions of compressing fluid

comp	Compressor
cooling	Cooling of external surface of compressor
DC	Direct current motor coil
DC,loss	DC motor losses
f	Fin measurement
fric	Friction
g	Gap from roller to chamber diameter
gap	Radial gap
h	Compressor chamber height
h,comp	length of fin along height of compressor
in	Inlet
l	Lubrication layer
leak	Radial leakage
Nu	Nusselt factor
oil	Conditions of lubricating oil
s	Conditions/measurements of steel
tot	Total
v	Vane
Vessel	Total volume of pressure vessel including tubing, tank and vacant area inside compressor casing
x	Subscript used if multiple value are calculated

1

INTRODUCTION

1.1. PROJECT CONTEXT

1.1.1. GLOBAL WARMING AND FOSSIL FUELS

The fact that global warming is progressing rapidly, is an undeniable fact [Hardy, 2003]. One of the biggest contributors to this climate change is the higher fraction of carbon dioxide in the atmosphere, creating the green house effect on the planet. The main reason for this higher carbon dioxide concentration is the burning of fossil fuels for energy by humans, which releases carbon dioxide. The scientific world is looking for alternatives to replace these fossil fuels as the main source of our energy on the planet. However, these alternatives do not cover all appliances where fossil fuels are used as the source of energy, for example: air travel, the creation of plastics and other scientific processes.

1.1.2. ZERO EMISSION FUELS

Fossils fuels cannot be easily substituted for other energy sources for some appliances. These hydrocarbons would still need to be extracted from the earth. The company Zero Emission Fuels is designing a solution to this problem. Zero Emission Fuels is designing a micro-plant which can create methanol from water and carbon dioxide in the air using the electricity produced by solar panels. The methanol can then be used as either a fuel for aircraft or as a component for scientific processes. By producing this methanol from the carbon dioxide in the air, the methanol would not increase the carbon dioxide concentration in the air when the methanol would be burned as a fuel. Hence the name of the company Zero Emission Fuels (ZEF).

THE MICROPLANT

ZEF made the decision to design a microplant that would be able to run on the electricity generated by 10 solar panels. This decision was made in order to be able to produce a large amount of microplants. Thereby, the cost of components needed for the microplant are also reduced, since it can then be mass produced. To convert the carbon

1

dioxide and water into methanol the microplant is divided into 4 sections shown in figure 1.1.

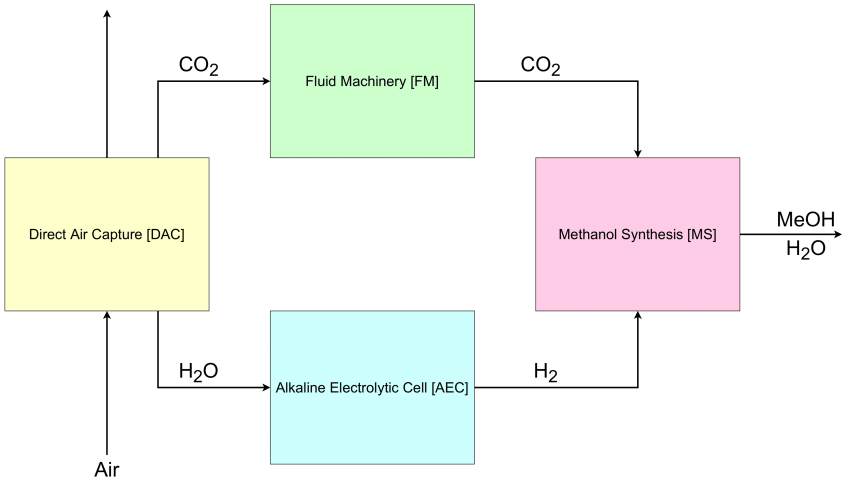

Figure 1.1: Process Flow Diagram of the ZEF Plant

Direct Air Capture First of all, the Direct Air Capture (DAC) captures the carbon dioxide and water from the ambient air. The carbon dioxide and water are then split into 2 seperate streams, where the water is in the liquid phase and the carbon dioxide is in the vapor phase.

Fluid Machinery The vapor stream from the DAC is fed into the Fluid Machinery (FM) section. Because the splitting of the carbon dioxide and water can not be done perfectly, there is also water vapor in the gaseous stream. Because the carbon dioxide will be compressed to 50 [bar], the water in the stream would be condensed into liquid water and could damage the compressor. Therefore the water is first extracted from the stream by letting it flow through a column filled with desiccant. Afterwards, the pure carbon dioxide stream is compressed with a compression train to 50 [bar]. During compression the lubrication of the compressor gets entrained in the flow and must therefore be separated from the carbon dioxide; using a fine stainless steel mesh after each stage. The pure high pressure carbon dioxide is then fed into the Methanol Synthesis (MS) section.

Alkaline Elektrolysis Cell Meanwhile, the liquid water stream from the DAC is transported to the Alkaline Electrolysis Cell (AEC) section. Here, the water is pressurized to 50 [bar] and is fed into a alkaline electrolysis cell to be split into oxygen and hydrogen. The oxygen is purged and the hydrogen is fed into the Methanol Synthesis (MS) section.

Methanol Synthesis In this section the high pressure hydrogen and carbon dioxide streams are combined and heated to produce the methanol. The efficiency of the MS is improved when the temperature and pressure are increased. This is the reason why the compressors in the previous system needed to compress the stream to high pressures.

1.1.3. COMPRESSION TRAIN REQUIREMENTS

This thesis will focus on the compression train in the Fluid Machinery section. For this compression train there are certain requirements that the compression train must meet to function properly inside the microplant.

Inlet conditions The inlet is assumed to be pure carbon dioxide at around 1 [bar] of pressure. The temperature of the stream depends on the ambient temperature. The ambient temperature will change depending on where the solar panels and microplant are placed in the world. Therefore the ambient temperature will vary between 10 and 40 [°C].

Outlet conditions The outlet pressure of the compression train is set to 50 [bar]. This is done due to the requirements for the efficiency of the Methanol Synthesis reactor which comes after the FM section.

Mass flow To feed enough carbon dioxide to the methanol reactor a mass flow of 336.7 [g/h] is needed. This constraint must be met to ensure the right molar balance with hydrogen inside the methanol reactor.

Life time Because the compressor is hermatically sealed it is not desirable to have to change components after some time. Therefore, the lifetime goal of the compression system is set to 20 years whilst operating 8 hours per day.

1.1.4. SCIENTIFIC RELEVANCE

Process intensification is an unbroken trend in chemical engineering [Grützner et al., 2018] and it can aid in discovering new innovative procedures to create renewable fuels and other chemical processes. A big trend in the process intensification is the use of micro-reactors and microplants to produce chemicals using small movable devices. For the smaller chemical plants most of the equipment needs to be scaled down. For most equipment in these microplants it is not difficult to achieve. However, because of the rotating parts of compressors this is more difficult. Mainly because of the increased surface area to volume ratio, which results in higher friction losses inside the system. The leakages inside the system are also increased when gas compressors are scaled down, thereby reducing the volumetric efficiency of the compressor. However, increased surface area to volume ratios do not only have negative effects. Due to the higher surface area to volume ratio, the heat transfer of the compressing fluid can be increased thereby allowing for the possibility of cooling of the compressed gas. In a normally scaled gas compressor the compression can usually be assumed to be adiabatic but the smaller compressors

might prove otherwise. This thesis was written with the purpose of assessing the positive and negative effects of scaling down a rolling piston compressor to produce low mass flows with high pressure differences.

1.2. RESEARCH QUESTIONS

The goal of this thesis is to design a carbon dioxide compression train for high pressures and low mass flows, using rolling piston compressors. Based on this goal, two research questions - together with several sub-questions - were formulated:

- What is the optimal amount of stages needed to compress carbon dioxide to high pressures with a low mass flow using rolling piston compressors?
  - What is the impact of the reduction/addition of stages on the thermodynamics of the compression?
    - What impact does the temperature of the fluid have on the life time of the lubricant?
    - What is the underlying thermodynamic process occurring in the rolling piston compressor, while the compressor operates within the operational parameters?
  - What is the impact of the reduction or addition of stages on the mass flow of the different compression stages?
    - Is the compression train able to reach the outlet pressure of 50 [bar] of the system?
    - How do the leakages scale for the different stages of the compressor?
    - How do the leakages scale with different rotational speeds?
  - What is the impact of the reduction or addition of stages on the power usage of the different compression stages?
    - How much do the friction losses impact the efficiency of the system?
- Is active cooling able to reduce the temperatures inside the compressor enough to operate the system with less compression stages?
  - How effective is the active cooling compared to the base compressor?

By answering these research questions, this thesis aims to find a first iteration of the ideal amount of compression stages and aims to highlight the areas which require further research.

1.3. PROJECT MILESTONES

To achieve the goal of constructing a compression train for this system, the following project roadmap was created, which includes important steps in the research to provide the final product of the compression train:

- Asses the options for active cooling using dimensionless analysis.

- Create computational model to calculate the inner workings of the compressor.
- Design a concept for the active cooling.
- Build an experimental setup to check calculated values with reality.
- Conduct the experimentation.
- Create conclusions and recommendations from the difference between the experimental data and the model.

1.4. PROJECT BOUNDARIES

There are many different types of compressors on the market and the amount of work that still needs to be done for the compression train is very large. Therefore this thesis has set up boundaries to bring the project to a more manageable size.

Pre and post treatment Before the carbon dioxide is fed into the compressor the carbon dioxide is first stripped of water. For this thesis, the stripping process is presumed to be an ideal process resulting in a inlet stream of pure carbon dioxide at a pressure of 1 [bar] of pressure.

After compression, the outlet stream contains a mist of lubricant. This lubricant is then separated from the stream. This separation needs to occur after every compression stage. This separation process is also assumed to be ideal: resulting in an outlet stream of the compression train consisting only of carbon dioxide.

Static operation Whilst the microplant is in operation, the DAC system has a dynamic outlet. This results in varying inlet conditions for the FM section. Therefore the compression train needs to be able to run at different rotational speeds to keep up with the DAC system. For this thesis, the inlet of the compression system is set as a static condition to make sure the scope of the thesis does not get too large.

Compressor type For this thesis, the only compressors that will be tested are the Purswave rolling piston compressors. The only measurement that will be changed in these compressors is the excenter of the crankshaft. In section 2.1 these decisions for the chosen rolling piston compressor are further explained.

Air instead of carbon dioxide Because carbon dioxide is a hazardous gas that causes suffocation in higher concentrations, all the experiments were conducted with ambient air instead of carbon dioxide.

Influence of lubrication flow For this thesis, the impact of the oil flow on the compression of the system is not taken into account. This was done to simplify the calculation for the pressures and the energy balances.

1

1.5. REPORT STRUCTURE

This thesis starts with addressing the relevant theory used for this project in Chapter 2. This Chapter is divided into three sections of theory. Chapter 2.1 reviews previous research done on the compression system. Chapter 2.2 goes into the thermodynamics of the compression, while Chapter 2.3 goes into the theory behind the leaks which occur during the compression and the heat produced by the DC motor and the friction in the compression chamber. In chapter 3 the method in which the research questions were put to the test is explained, starting with the computational model in chapter 3.1 and the experimental method in chapter 3.2. The results from this method are explained in chapter 4, together with a discussion on the results. Afterwards, the conclusions from the research are presented in chapter 5. Finally, the recommendations for further research into the topic of this thesis are presented in chapter 6.

2

THEORY

In this chapter the relevant theory for this research is set out in the three following sections:

- 2.1 Prior research into the compression system
- 2.2 Dimensionless Analysis
- 2.3 Mechanical Design

2.1. PRIOR COMPRESSOR RESEARCH

Before the start of this thesis, previous research into the compression system for low mass flows and high pressure differences was already conducted. This research focused on what compressor type would be best, how the chosen compression type worked and how these compressors could be adapted to function better for the constraints set for the system.

2.1.1. COMPRESSOR TYPE

One of these previous researches focused on what compressor type would perform best for the constraints for the system by [de Koning, 2020]. This research concluded that the best option for this compression system would be a compression system without lubrication. An oil lubricated compressor was concluded to be the runner up. However, the drawback of compressors without lubrication was that there were no compressors of that type on the market. Therefore, this thesis will be focused on oil lubricated compressors, which are available on the market. The compressor type that was already on market was a rolling piston compressor. Because this is the only compressor on the market this thesis will only look at rolling piston compressors.

2.1.2. ROLLING PISTON COMPRESSOR

The author of this thesis did part of the prior research into the compression system. The next section explains the workings of the rolling piston compressor and is also men-

tioned in his internship report [Bergstein, 2020].
The rolling piston compressor is a simple compressor that compresses a medium through the rotation of a roller (white ring in figure 2.1) which is turned by an eccentric crankshaft (inner grey circle in figure 2.1.) The compressor has 2 modes: "Suction mode" and "Compression mode". Each mode is separated by the vane (which is positioned on the top of the compressor in figure 2.1) and the small gap in between the roller and the compressor housing (The outer grey ring in figure 2.1). The vane is pushed against the roller with a pre-loaded spring. The small gap in between the roller and the compressor housing is sealed with the lubrication of the compressor to create two leak tight chambers, in which the suction and compression can take place.

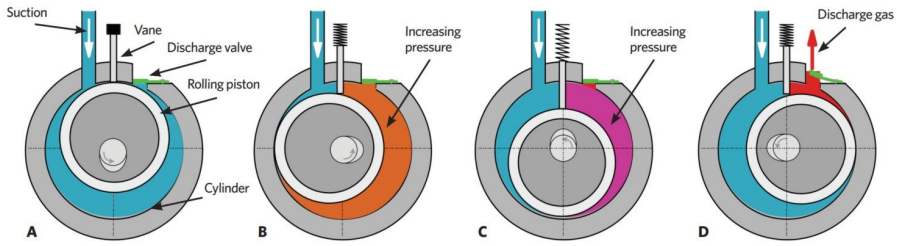

Figure 2.1: A simplified view of the operation of a rolling piston compressor [Dwyer, 2020]

Suction In figure 2.1 the compressor starts at position A. In this position there is no pressure in the system and the inlet and outlet are connected. The outlet is however closed due to the pressure outside of the cylinder, which pushes against the valve thereby closing it. The roller is then turned in a counter clockwise direction towards position B. Here the compressor starts sucking from the inlet. The compressor keeps turning to position C and then D, to eventually come back to position A. This completes the suction cycle. The cycle is stopped once the roller reaches the vane on the top of the compressor, like in position A. In this position the compressor has taken in its maximum amount of gas from the inlet.

Compression The compression cycle starts when the roller passes the inlet port. The compressor turns from position A to B and keeps rotating to C and then D. Once the pressure inside the compression chamber is above the pressure after the valve of the outlet of the compressor, the valve opens as seen in position D. Then the gas is pushed through the valve. This is done until the pressure inside the chamber is not higher than the pressure after the valve. Then the valve closes again and the compressor turns to position A to start a new suction cycle.

Lubrication of the compressor To ensure the compressor does not leak at the gap between the roller (#4 in figure 2.2) and the top and bottom flanges (#1 & #6 respectively)

and between the roller and the compressor housing (#7), The gaps are filled with lubricant. This lubricant also ensures that the wear of the compressor is minimized. At every rotation, a small amount of lubricant is discharged through the valve of the compressor (#2). To replenish the lubricant which was lost, the compressors have a built in lubricant reloop. The compressor is positioned in a reservoir of lubricant. This reservoir is the empty space between the outer shell of the compressor and the inner parts which can be seen in figure 2.2. There is a hole in the crankshaft with a coiled plate (#5) in it, which scoops up lubricant from the reservoir. Because the crankshaft is turning very fast, the lubricant gets swung to the edge of the hole. This pushes the lubricant through the holes on the side of the crankshaft. These holes can be seen on the crankshaft in figure 2.3. The lubricant is now lubricating the roller and the crankshaft. The lubricant is slowly spun outwards in between the roller and the flanges, before it ends up inside the compression chamber and until it is flung out of the compression chamber when the valve is opened during the discharge of the pressurized fluid.

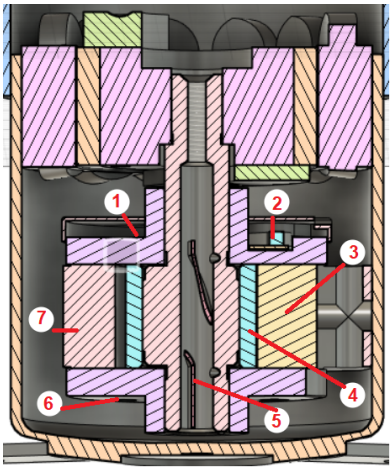

Figure 2.2: The disected view of the Purswave compressor.

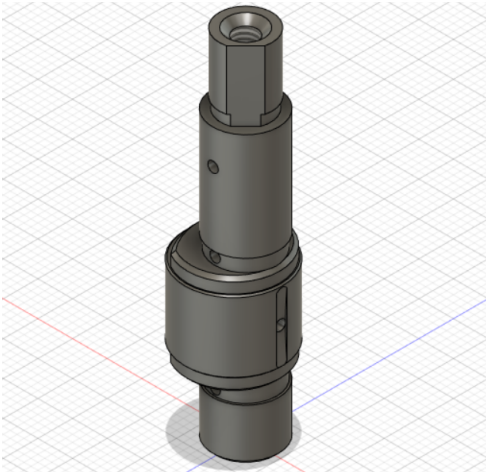

Figure 2.3: Purswave compressor eccentric crankshaft.

2.1.3. ASPEN & PURSWAVE COMPRESSORS

The rolling piston compressor which was available on market was designed by Aspen Compressors. This compressor is currently hailed as the smallest refrigeration compressor in the world. The small displacement volume of these compressors resulted in a very low mass flow, which almost met the constraints of the compression system requirement for the compression system. However, if the compression were to have more than 1 stage, the volumetric flow rate would become too big. Therefore, adjustments would have to be made to the compressor. The Aspen compressors are however very expensive. Because multiple prototypes would need to be made of the compressors, a cheaper alternative was needed, which was produced by the company Purswave. These compressors were disassembled and the inner parts of the compressor were salvaged to be

used in the modular compressors used for this research. The inner parts include the numbered components in figure 2.2, together with the rotor and stator of the DC motor, which provides torque to the compressor. The rotor and stator are the components which are depicted above the numbered components in figure 2.2. The Purswave compressor has a displacement volume of 1.9 [cc] and a rotational speed of 2000 to 6000 [RPM]. The lubricant prescribed by Aspen was Emkarate RL68H. Due to the similarity of the compressors, this lubricant is also used for the Purswave compressors. This lubricant has a high thermal stability: up to 175 [°C] and higher [Parker, 2012]. For this thesis the maximum temperature which the lubricant can reach is however set to 100 [°C] because, while it can function at higher temperatures, Aspen Compressors advised that the temperature should not exceed 100 [°C].

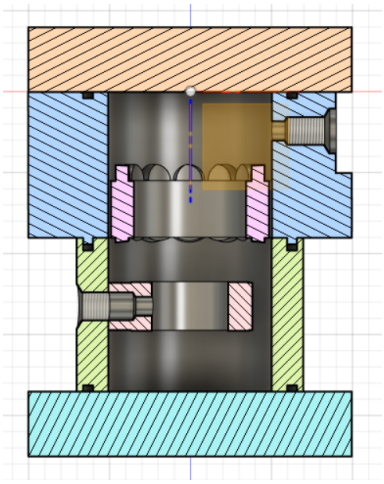

Figure 2.4: The housing of the modular compressor.

2.1.4. MODULAR COMPRESSORS

The compressors from Purswave are hermatic compressors, in which the hull of the compressor is sealed. To make testing with the compressors easier, ZEF started building modular compressors. A cross sectional view of the modular compressor is visible in figure 2.4. This was done to ensure easy assembly and subsequent disassembly, in case parts needed to be changed. The modular compressor housing consisted of 4 parts from top to bottom:

- Top lid (orange)
- Motor casing (blue with motor coil (pink) inside)
- Chamber casing (green with chamber (orange) inside)
- Bottom lid (turquoise)

These 4 parts can be clamped together to create a leak tight seal. The seal is provided with an o-ring inside the groves in between the different parts. Also the motor casing has an extrude which fits inside the grove of the compressor chamber casing. This ensures that the motor and compression chamber are perfectly aligned. The Purswave compressor has a displacement volume which would fit well as a first stage for the compressor. However, if the compression would consist of more than 1 stage, the later stages would need reduced displacement volumes. This is caused by the compression of the gas in the first stage, which results in a lower volumetric flow while the mass flow stays constant. To decrease the compressor volume, two alternatives were investigated. The first alternative is to reduce the height of the compression chamber. The second alternative is to reduce the excenter of the crankshaft while increasing the roller diameter. First an attempt was made to create a compressor with a reduction in height. This resulted in a compression chamber housing that leaked. When the height of the compression chamber was reduced, it became clear that the equipment needed to ensure the correct measurements was not available at the faculty. Therefore, the decision was made to only change the inner parts of the compression chamber to ensure no leakages in the compressor chamber housing [Bergstein, 2020].

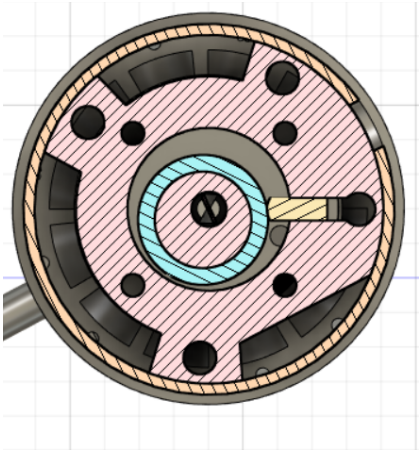

Figure 2.5: Top view of Purswave compressor with original excenter and roller

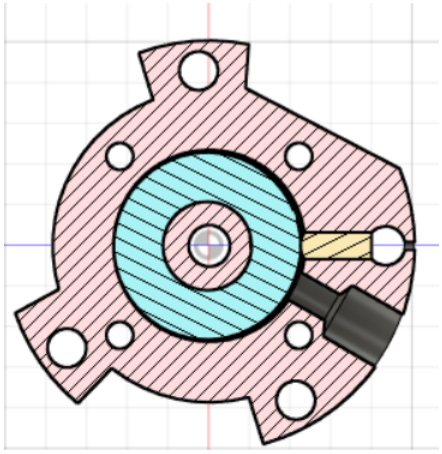

Figure 2.6: Top view of Purswave compressor with adjusted excenter and roller

When the excenter of the crankshaft is reduced, the roller inside diameter decreases while the external roller diameter increases; resulting in a larger roller. This is visible when comparing the original Purswave roller (blue) in figure 2.5, with the adjusted roller (blue) in figure 2.6. When comparing figures 2.5 & 2.6 the area in between the roller (blue) and the compressor housing (outside red) is decreased dramatically. The height of the displacement volume is the same in both cases because the compressor housing is not changed. This results in a smaller displacement volume for the adjusted excenter and roller.

2.2. DIMENSIONLESS ANALYSIS

This section is written with the goal of getting a better idea of how much heat is created by the compression of the carbon dioxide and what concepts of cooling can be used to mitigate the heating of the lubrication.

2.2.1. POLYTROPIC COMPRESSION

When a gaseous fluid is compressed in a compressor, the compression generally occurs adiabatically. This means that the heat created by the compression is not dissipated to its surroundings during compression. This would result in high output temperatures for a compressor if the pressure ratio is high. These outlet temperatures can be calculated using the equation 2.1 for constant specific heats from [Moran et al., 2012]. Important to note is that the assumption of constant specific heat is not valid, as will be further explained in chapter 2.3.2. Because this calculation is made to get a rough idea of what is happening, the assumption is used nonetheless. Here γ represents the polytropic coefficient. For adiabatic compression the polytropic coefficient is equal to the ratio of specific heats, which is 1.297 for carbon dioxide at a pressure of 1 [bar] and a temperature of 20 [°C] [NIST Standard Reference Database, 2010]. The outlet temperatures for the different pressure ratios, which belong to a different amount of stages used for the compression train, are shown in table 2.1.

$$T_2 = T_1 \left(\frac{p_2}{p_1} \right)^{\frac{\gamma-1}{\gamma}} \tag{2.1}$$

Number of stages	1	2	3	4
Pressure ratio [-]	50	7.07	3.68	2.66
Temperature [K]	717	458	395	366
Temperature [°C]	442	183	119	91.5

Table 2.1: Outlet temperatures for different pressure ratios assuming adiabatic compression

From the values in table 2.1 can be concluded that the compression train would need to consist of at least 4 stages to ensure the temperature does not exceed the limit of the lubricant. However, this is probably not the case. That is because the compression is assumed to be adiabatic, which is not necessarily true. The phenomenon in which the polytropic coefficient is equal to 1, is called isothermal compression. When this happens the compression loses all its heat of compression to its surroundings. Because there can never be perfect thermal isolation of the system, the polytropic coefficient will probably lie somewhere between 1 and the ratio of specific heats. The polytropic coefficient of the compression process in this thesis is not yet known. This will be examined in chapter 3 & 4. A lower polytropic coefficient would mean a lower compressor outlet temperature. But this might also not be the case, because in the current calculation the heat production of friction and the DC motor are not taken into consideration. The friction and DC motor heat production will be examined further in chapter 2.3.

2.2.2. ACTIVE COOLING CONCEPTS

The amount of stages of the compression train would preferably be kept as low as possible to reduce the cost of the system. Another consequence of more stages would be that the leakages inside the compressor increase. This will be further examined in chapter 2.3. To decrease the amount of stages, the exit temperature after compression would need to be decreased. To achieve this two concepts for the active cooling of the compressor were devised.

Atomization of lubricant The first concept was that the lubricant inside the compression chamber would get entrained into the flow of carbon dioxide in very tiny droplets (a mist). The heat capacity of the compressed fluid would increase significantly, thereby reducing the temperature rise of the compressed carbon dioxide [Kremer et al., 2012]. The heat capacity of the fluid would increase because the lubricant which is dispersed as a fine mist inside the fluid has a much higher heat capacity than the carbon dioxide. Also, because the lubricant is mixed isotropically (evenly distibuted) through the fluid in small droplets, the area available for heat transfer is increased dramatically; making it easier for the compressing fluid to release its heat. This results in a lower polytropic coefficient. However, before this concept can be implemented, a dimensionless analysis must be done to evaluate whether the lubricant is dispersed in a fine mist during compression. This will be done in chapter 2.2.3. Because the lubricant gets entrained into the fluid, more lubricant is lost every cycle of the system.

Cooling through compressor housing If the lubricant does not get entrained into the fluid and sticks to the walls of the compression chamber, the lubricant might be cooled through the compressor housing. This can be achieved only if the conductive heat transfer through the body of the compressor housing and lubrication layer is much greater then the convective heat transfer from the compressed fluid to the lubrication layer. This way, the cold lubricant outside of the compressor housing can extract more heat from inside of the compressor, ensuring a cooler lubricant. In chapter 2.2.3 an analysis is done whether this can be assumed to work for this system.

2.2.3. ANALYSIS

A dimensionless analysis is useful to get a better idea of what the dominant phenomena are inside the system. A dimensionless analysis is done by estimating some values and simplifying them. These values are inserted into formulas for dimensionless numbers to get an idea of what phenomena are dominant. This makes the calculations easier and gives a good estimate of what is happening. To examine whether the concepts mentioned before in chapter 2.2.2 are implementable a dimensionless analysis will be used. Each dimensionless number is assessed for 1, 7.07 and 50 [bar] for the Purswave compressor in figure 2.5. The Purswave compressor gives a good indication for the dimensions needed for the first compression stage. 1 [bar] would relate to the inlet of the compressor while 7.07 [bar] would be for the outlet of a two stage compression train while 50 [bar] would be for the outlet of a single stage compression train. The adjusted compressor shown in figure 2.6, gives a good indication of the dimensions needed for the second stage for the compression train. Therefore, the inlet conditions are assessed at a

pressure of 7.07 [bar] and the outlet conditions at 50 [bar]. The temperature for the inlet is assumed to be 20 [°C] while the temperature for the outlet is assumed to be 100 [°C]. Both compressor measurements were tested for different rotational speeds. This was done because the dimensionless numbers are both influenced by the speed at which the compressor runs. The speeds examined were the minimal and maximum rotational speed of the compressor, being 2000 and 6000 [RPM] respectively.

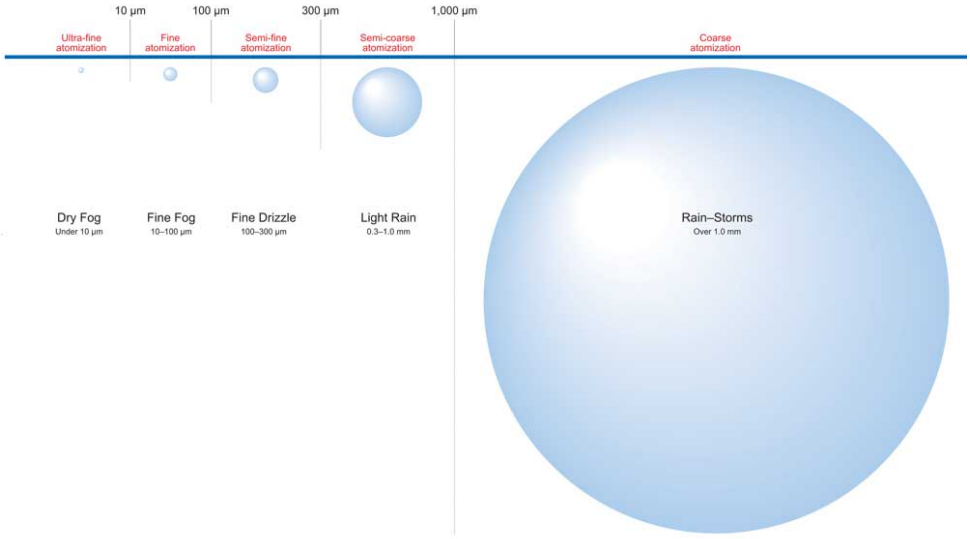

Figure 2.7: Indication of droplet sizes taken from [Ikeuchi Europe, 2019].

ATOMIZATION OF LUBRICANT

To asses whether the concept for the atomization of the lubricant works, the Weber number is investigated for this system. The size of the droplets inside the compressor must be calculated. The average droplet size assumed by [Kremer et al., 2008] for their system was 1.4 [μm]. However the atomization of the lubricant was done with a nozzle. With a nozzle, the droplet size can be controlled better. This is not the case for our system. Therefore the droplet size goal was set lower at 10 [μm] which is characterized as the limit for "Ultra fine atomization" or "Dry fog" in figure 2.7. To asses whether the droplet breakup inside the compressor creates droplets that are small enough, normally the Weber number is used. The Weber number (equation 2.2) relates the inertia force of the fluid against the surface tension forces. However, in this equation the viscosity effects inside of the droplets are not taken into account. To take these effects into account the Ohnesorge Number (equation 2.3) is also calculated [Majithia et al., 2008].

$$We = \frac{\rho_{CO_2} u^2 D_d}{\sigma} \tag{2.2}$$

$$Oh = \frac{\mu}{\sqrt{D_d \rho_{oil} \sigma}} \tag{2.3}$$

For each Ohnesorge number, a critical Weber number is calculated according to figure 2.8.

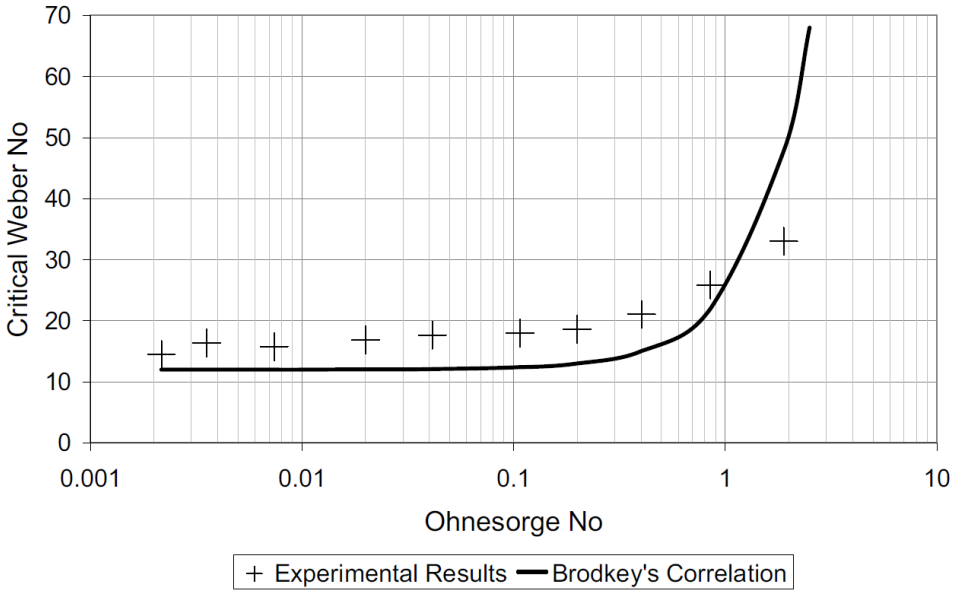

Figure 2.8: Variation of Critical Weber Number with Ohnesorge Number taken from [Majithia et al., 2008]. A curve was fitted to the experimental results of this figure to calculate the critical Weber number for each droplet size.

σ = **surface tension [N/m]** The surface tension of the lubricant "emkarate RL68H" is assumed to be 0.0286 [N/m]. This estimate comes from the static surface tension test results from [Goswami et al., 1997].

ρ = **density** [kg/m^3] The density for the CO_2 is extracted from REFPROP [NIST Standard Reference Database, 2010]. While the density for the oil is 977 [kg/m^3] which is taken from the data sheet of the oil.

μ = **dynamic viscosity [Pa/s]** The dynamic viscosity for the oil is 0.19 [Pa/s] at the inlet conditions and 0.0027 [Pa/s] for the outlet conditions which are calculated from the data sheet of the oil.

$$u = \omega r = 2\pi \frac{RPM}{60} \frac{D_c - L_g}{2} \tag{2.4}$$

u = **tangential velocity [m/s]** The velocity in the formula for the Weber number (equation 2.2) is the tangential velocity of the roller at the middle of the maximum gap size (equation 2.4). This can be calculated by subtracting the diameter of the compressor chamber [D_c] with the maximum gap size [L_g] and dividing them by 2 to get the radius. However, this only applies for the inlet of the compressor. For the outlet, the maximum gap size is estimated to be smaller because the higher pressures of the outlet are only achieved when the rolling piston compressor has executed around 75% of its revolution (position D in figure 2.1). When comparing the channel width of the high pressure condition (position D in figure 2.1) with the channel width at the low pressure condition (position A in figure 2.1), it is clear that the width has decreased. How much exactly is not known, but the estimate is made that the maximum gap size of the outlet is $L_{g,out} = L_{g,in}/2$. The RPM is multiplied with 2π and divided by 60 [s] to convert it to [rad/s].

D_d = **droplet diameter [m]** To asses at what droplet diameter the droplets would stop breaking up, different droplet diameters were checked after each other from $D_d = 1$ [μm] to $D_d = 1000$ [μm] with steps of 1 [μm]. The Weber number was calculated using equation 2.2 and the critical Weber number was calculated using the Ohnesorge number from equation 2.3 and a fitted curve from the experimental data from figure 2.8. Afterwards, the droplet diameter at which the Weber number and the critical Weber number are closest to each other is assumed to be the final droplet diameter after droplet breakup. If the outcome is a droplet diameter of 1000 [μm], then the diameter is assumed to be $D_d >$ 1000 [μm]. The limit is set at 1000 [μm] because the heat transfer is a lot less effective when the droplet diameter increases and after this point the atomization of the lubricant will have almost no effect.

Results When looking at the results for the droplet diameters in table 2.2 & 2.3 it is clear that the droplets do not reach the desired droplet diameter. This means the lubricant will probably not cool the stream of carbon dioxide enough. Therefore, it can be stated that it is probably not worthwhile to elaborately test this method of cooling.

COOLING THROUGH COMPRESSOR HOUSING

To compare the heat transfer through the compressor housing and lubrication layer with the heat transfer from the fluid to the lubrication layer, the Biot number can be examined (equation 2.5). This formula relates the convective heat transfer of the fluid against the conductive heat transfer of an object as is depicted in figure 2.5. When $Bi << 1$ the compressor housing conducts the heat very well compared to the fluid inside the housing. This would mean the temperature outside of the housing would be about the same as the temperature on the inside. That means that to cool the fluid properly, the outside temperature does not have to compensate its heat transfer properties by reducing in temperature. When $Bi >> 1$ there exists a large temperature gradient inside the compressor housing. This means the heat produced by the compression is not extracted through the housing very well. That would have resulted in a very low temperature outside of the

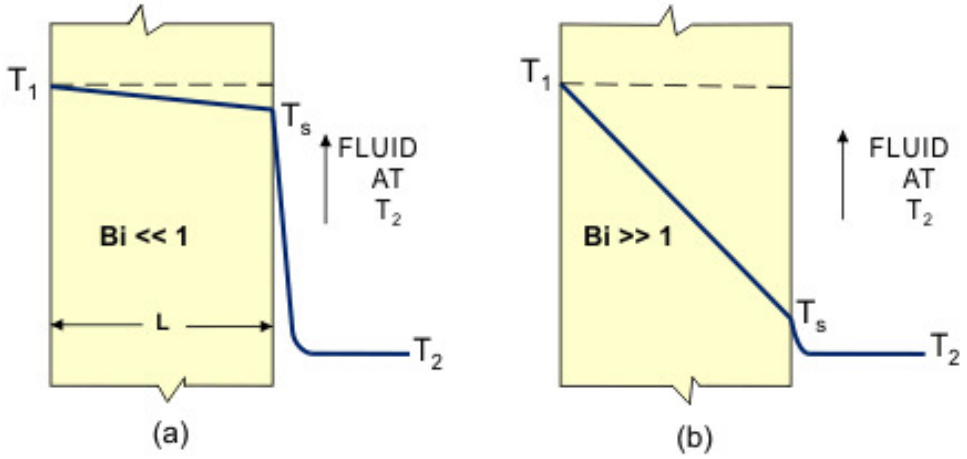

Figure 2.9: Comparison of fully developed temperature profiles in two plates cooled by the same fluid [Thermopedia, 2011]. On the left side the heat is conducted very well through the wall while the left side conducts the heat worse.

compressor if the same amount of heat needed to be extracted as when $Bi << 1$.

$$Bi = \frac{h_{CO_2}}{k_{avg}} L_h \tag{2.5}$$

L_h **= Length of compressor housing + lubrication layer [m]** In equation 2.5, $L_h = L_s + L_l$ is the thickness of the compressor housing $L_s = 0.75$ [cm] and the lubrication layer thickness together. The Biot number will be assessed for 3 thicknesses of the lubrication layer: no lubrication layer; 20 [μm]; and 100 [μm]. The instance with no lubrication layer is assessed to see how well the heat is transferred through the compressor housing. The 20 [μm] thickness would occur when the leakage gap between the roller and the excenter housing is ideal. However, such a small gap is hard to produce due to the tight tolerance needed. When this thesis started, the minimal leakage gap that was constructed was around 100 [μm], therefore this minimal gap size between roller and compressor housing is also examined. Important to note is that the cylindrical shape of the compressor housing has not been taken into account and the calculation is done in an 1 dimensional space. If it were taken into account the equation would be formulated like equation 2.23.

$$\Sigma R = R_s + R_l = \frac{L_s}{k_s A} + \frac{L_l}{k_l A} = \frac{L_s + L_l}{k_{avg} A} \Rightarrow k_{avg} = \frac{L_s + L_l}{\frac{L_s}{k_s} + \frac{L_l}{k_l}} \tag{2.6}$$

k_{avg} **= average thermal conductivity of the compressor housing + lubrication layer [W/mK]** The average thermal conductivity of the compressor housing together with the lubricant is calculated with equation 2.6, taken from [Mills, 2014]. Here the thermal resistances of the compressor housing and lubricant are added together to get the to-

tal thermal resistance. By rewriting the formula, the average thermal conductivity can be calculated. In this formula L_s is the thickness of the compressor housing and L_l is the thickness of the lubrication layer. $k_s = 58$ [W/mK] is the thermal conductivity of carbon steel at 100 [°C] according to [Sinnott and Towler, 2013]. The thermal conductivity of the lubricant emkarate RL68H is assumed to be roughly the same as the conductivity of another POE oil mentioned in [Bruno et al., 2019]. At 158 [°C] and 1.01 [bar] $k_s = 0.129$ [W/mK] for this POE oil. At the same temperature but for 62 [bar] $k_s = 0.132$ [W/mK]. Because these values are not far apart the thermal conductivity was estimated to be $k_s = 0.130$ [W/mK] for all pressures.

$$Nu = \frac{h_{CO_2} L}{k} \Rightarrow h_{CO_2} = \frac{Nu}{L_g} k_{CO_2} \tag{2.7}$$

h_{CO_2} = **Convective heat transfer coefficient of the fluid** [W/m^{2}K] The heat transfer coefficient of the carbon dioxide is calculated by rewriting the formula the Nusselt number (equation 2.7). Here L_g is again the gap size like in equation 2.4. k_{CO_2} is the thermal conductivity of carbon dioxide which is calculated using REFPROP [NIST Standard Reference Database, 2010].

$$Nu = 0.092(TaPr)^{\frac{1}{3}} \tag{2.8}$$

Nu = **The Nusselt number for a Taylor-Couette flow [-]** Since the fluid is flowing around a smaller cylinder inside a bigger cylinder, the flow inside the compressor is assumed to be a Taylor-Couette flow. For a Taylor-Couette flow, the Nusselt number can be estimated using equation 2.8 from [Tachibana and Fukui, 1964]. Here the Prandtl number [Pr] is calculated using REFPROP [NIST Standard Reference Database, 2010].

$$Ta = \frac{\omega^2 r_1 (L_g)^3}{\nu^2} \tag{2.9}$$

Ta = **Taylor number for the flow in between the roller and compressor housing [-]** The Taylor number is calculated using ω which is the same as in equation 2.4. L_g is again the same gap size as in equation 2.4 & 2.7. ν is the kinematic viscosity of carbon dioxide calculated with REFPROP [NIST Standard Reference Database, 2010]. r_1 is the radius of the inner cylinder (equation 2.10). Here the compressor chamber diameter [D_c] & gap size [L_g] are the same as in 2.4

$$r_1 = \frac{D_c}{2} - L_g \tag{2.10}$$

Results The results of the dimensionless numbers were plotted in table 2.2 & 2.3. Bi << 1 was valid for most conditions. However the Biot number got closer to 1 when the lubrication layer was equal to $L_l = 100$ [μm]. It is clear that when the minimal gap of the compression housing is reduced to 20 [μm], which in turn reduces the thickness

RPM	p [bar]	D_d [μm]	Ta [$*10^6$]	Nu	$Bi_{0\mu m}$	$Bi_{20\mu m}$	$Bi_{100\mu m}$
2000	1	>1000	0.285	5.53	0.00310	0.00678	0.0215
	7.07	>1000	0.427	6.26	0.0127	0.0277	0.0879
	50	>1000	22.6	23.9	0.0511	0.112	0.355
6000	1	>1000	2.56	11.5	0.00644	0.0141	0.0447
	7.07	>1000	3.84	13.0	0.0263	0.0576	0.183
	50	155	203	49.7	0.106	0.233	0.738

Table 2.2: Dimensionless numbers for the Purswave compressor for different pressures and different RPM.

RPM	p [bar]	D_d [μm]	Ta [$*10^6$]	Nu	$Bi_{0\mu m}$	$Bi_{20\mu m}$	$Bi_{100\mu m}$
2000	7.07	>1000	0.169	4.71	0.0134	0.0292	0.0928
	50	>1000	0.211	5.04	0.0535	0.117	0.372
6000	7.07	>1000	1.52	9.80	0.0278	0.0608	0.193
	50	136	1.90	10.5	0.111	0.244	0.774

Table 2.3: Dimensionless numbers for the adjusted compressor for different pressures and different RPM.

of the lubrication layer to the same thickness, the conductance of the compressor housing is improved by a factor 3. Therefore it is important to seek small tolerances for the compressor gap. The Biot number also got closer to 1 when the pressure of the system was 50 [bar]. This would mean that the conductivity of the casing is getting closer to the convective heat transfer of the fluid. However, the Biot number does stay below 1. As a conclusion, more research into the concept of "Cooling through compressor housing" would be very valuable. The concept of cooling the compressor will be put to the test in chapter 2.3.

2.3. MECHANICAL DESIGN

In this section, the decisions for the mechanical design of the compression train are explained together with the mechanical phenomena that are important to examine for the system. Also, a first attempt is made to asses the energy and mass balance of the compression train. Next, the leakage rate inside each compressor will be researched in section 2.3.2. With more knowledge on the leakage rate inside the compressor, a better understanding can be established on what the pressure inside each compressor is during the rotation of the roller together with the mass flow produced by the compressor. Afterwards, the lubricant flow through the compressor is modelled to examine how much heat is extracted from the flow through the lubricant in section in section 2.3.3. To complete the heat production of the system, the compressor losses are calculated in section 2.3.5. Finally, the thermal resistance scheme of the compressor is evaluated to be able to calculate the effectiveness of active cooling for the compression train. These calculations are all merged in a computational model to be able to get a first glimpse of what is happening inside the compressor during operation. The computational model is further

explained in chapter 3.1.

2.3.1. MASS & ENERGY BALANCE

The mass balance was first defined with equation 2.11. Here, the incoming masses are on the left side of the equation and the outgoing masses are on the right side. Once the compressor reaches steady state the flows into and out of the system also balance out.

$$\begin{aligned} \dot{m}_{CO_2,in} + \dot{m}_{oil,in} &= \dot{m}_{CO_2,out} + \dot{m}_{CO_2,leak} + \dot{m}_{oil,out} \\ \Rightarrow \dot{m}_{CO_2,in} &= \dot{m}_{CO_2,out} \;\&\; \dot{m}_{oil,in} - \dot{m}_{CO_2,leak} = \dot{m}_{oil,out} \end{aligned} \tag{2.11}$$

Because these flows balance out, the flows are called the same on each side of the equation in equation 2.12. Here the compressor power together with the losses of the compressor and the increase in enthalpy of the oil and CO_2 result in the energy balance of the system.

$$\dot{m}_{CO_2} h_{CO_2,1} + \dot{m}_{oil} h_{oil,1} + W_{comp,tot} = \dot{m}_{CO_2} h_{CO_2,2} + \dot{m}_{oil} h_{oil,2} + Q_{fric} + Q_{DC,loss} \tag{2.12}$$

2.3.2. PRESSURE INCREASE DURING ROTATION

To calculate the pressure inside the compressor during a single revolution, first the assumption was made that the compression process is an isentropic process with constant specific heats. This was done because the differences in specific heats for the inlet and outlet were not that big (max 4.25%) as is visible in table 2.4. As is also visible in this table, the same assumption cannot be made for CO_2 since there the specific heat do not stay constant. To calculate the pressure equation 2.13 from [Moran et al., 2012].

$$\frac{p_2}{p_1} = \left(\frac{v_1}{v_2}\right)^{\gamma} \tag{2.13}$$

		Air		CO_2	
System	Stage	C_v	C_p	C_v	C_p
2 stage	1	3.89	2.89	22.5	17.9
	2	4.25	3.73	23.9	20.8
3 stage	1	1.74	1.32	14.8	11.7
	2	1.82	1.55	15.2	12.6
	3	2.08	2.21	15.9	13.2

Table 2.4: The difference of specific heats between the inlet and outlet of each compressor in percentages. The assumption of constant specific heats can be applied for air but not for CO_2 since with CO_2 the specific heats change too much.

COMPRESSION CHAMBER VOLUME

Due to the rotation of the crankshaft the volume of the compression chamber is changed, leading to the increase of pressure. The volume of the compression chamber and the

vane are calculated according to the formulas in equation 2.14 & 2.15 respectively [Subiantoro and Ooi, 2019].

$$V_{\text{chamber}} = \frac{R_c^2 L_h}{2}\left[\left(1-\Upsilon^2\right)\theta - \frac{(1-\Upsilon)^2\sin 2\theta}{2} - \Upsilon^2\sin^{-1}((\Upsilon-1)\sin\theta) - \Upsilon(1-\Upsilon)\sin\theta\sqrt{1-(\Upsilon-1)^2\sin^2\theta}\right] \tag{2.14}$$

$$V_{\text{vane}} = \frac{R_c L_h t_v}{2}\left[1-(1-\Upsilon)\cos\theta - \sqrt{(1-\Upsilon)^2\cos^2\theta + 2\Upsilon - 1}\right] \tag{2.15}$$

here:

- θ is the rotor's angular position.
- $\Upsilon = \frac{R_r}{R_c}$ is the ratio between the rotor and the cylinder radii.
- L_h is the chamber height.
- R_c is the cylinder radius.
- R_r is the rotor radius.
- t_v is the vane thickness.
- V is volume.

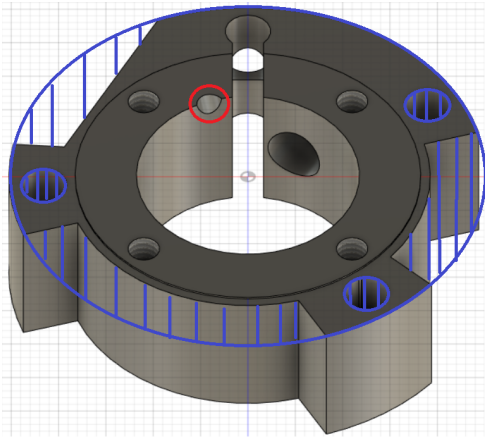

Figure 2.10: The outlet slot of the valve in the compressor housing indicated with the red circle and the empty spaces of the compressor housing which is assumed to be filled with steel as mentioned in chapter 2.3.6.

The paper of [Subiantoro and Ooi, 2019] then calculates the volume of the compression chamber by subtracting the vane volume from the compression volume. However,

this calculation does not incorporate the existence of the dead volume inside the compressor. For this compressor, the dead volume is located at the encircled part of figure 2.10. This space is created to free up space for the flow through the valve on top of the slot. This volume is measured to be: $V_{dead} = 3.53$ [mm^3]. The dead volume is added to the existing formula from [Subiantoro and Ooi, 2019] in equation 2.16 which is used to calculate the volume of the compression chamber during rotation.

$$V_\theta = V_{chamber} - V_{\text{vane}} + V_{dead} \tag{2.16}$$

RADIAL LEAKAGE

During rotation, the pressure inside the compression chamber increases. The compression chamber and suction chamber are connected with each other through the small radial gap. Because of the pressure difference between the two chambers fluid will leak from the compression chamber to the suction chamber. The rate at which this leakage occurs (equation 2.17) is assumed to be somewhat similar to the leakage rate described in [Kim et al., 2016].

$$\dot{m}_{leak} = f_{leak} A_{gap} \left(p_2 - p_1\right) \sqrt{\frac{M}{RT_{in}}} \tag{2.17}$$

Here, the leakage flow was estimated to be a compressible orifice flow. After modelling the equations used in [Kim et al., 2016] the leakage rate was not comparable to the results gathered from previous experiments. Therefore the equation was simplified to only be dependent on the area of the gap in between the two chambers and the pressure difference between the two chambers. Afterwards, no difference between chocked and non chocked flow was taken into account. With the results from previous experiments the leakage factor (f_{leak}) was calculated. This was done by incrementally increasing the leakage rate from 0 with tiny steps. The maximum pressure which the Pursewave compressor could achieve from ambient conditions was 30 [bar]. For each leakage rate, a single revolution of the roller was performed. Once the pressure inside the compressor did not go above 30 [bar], the leakage rate was set to the leakage rate which the last iteration of the loop had.
Equation 2.13 can be rewritten to be able to calculate the pressure inside the compression chamber with internal leakages.

$$\left(\frac{v_1}{v_2}\right)^\gamma = \left(\frac{n_2}{n_1}\frac{V_1}{V_2}\right)^\gamma = \left(\frac{m_2}{m_1}\frac{V_1}{V_2}\right)^\gamma \tag{2.18}$$

First the partial molar volume is rewritten as the compressor volume is divided by the amount of moles in the chamber. The ratio of molar amounts can then be rewritten as the ratio of the mass inside the compression chamber. Here m_1 is the mass of fluid inside the compressor when the compressor roller is at the start of the cycle and the compressor volume is at its maximum. While m_2 is the mass left inside the compression chamber after leakage. Using this relation equation 2.19 is formed and can be used to calculate the pressure inside the compression chamber during the rotation of the roller.

$$p_2 = p_1 \left(\frac{m_2}{m_1}\frac{V_1}{V_2}\right)^\gamma \tag{2.19}$$

VALVE THROUGHPUT

Once the pressure inside the compression chamber is higher than the pressure outside of the compressor, the valve will open and mass is transferred from the compression chamber to the casing of the rolling piston compressor. The amount of mass that is passed through the valve is calculated by assuming the pressure inside the compression chamber will become equal to the pressure outside the compression chamber. Afterwards, the amount of mass left inside the compression chamber can be calculated using equation 2.20.

$$\frac{p_3}{p_2} = \left(\frac{V_3}{V_2}\frac{m_3}{m_2}\right)^{\gamma} \Rightarrow m_3 = m_2\left(\frac{p_3}{p_2}\right)^{\frac{1}{\gamma}} \tag{2.20}$$

During the calculation of equation 2.20 the compressor is not moving. Therefore there is no volume change resulting in: $V_3/V_2 = 1$. p_2 & m_2 are the pressure and mass of fluid inside the compressor before the discharge occurs. p_3 is the pressure outside of the compression chamber and m_3 is the mass left inside the compression chamber after discharge.

2.3.3. OIL FLOW

Before a good estimation for the mass and energy balance of the compressor can be made, the oil flow though the compressor needs to be estimated. The oil flowing through the compressor is important to lubricate the contact surfaces that move at high velocities over one another. This prevents the wear of the compressor. To estimate the oil flow a model was made by [Padhy, 1994]. This model is used to model the oil flow inside the compressor.

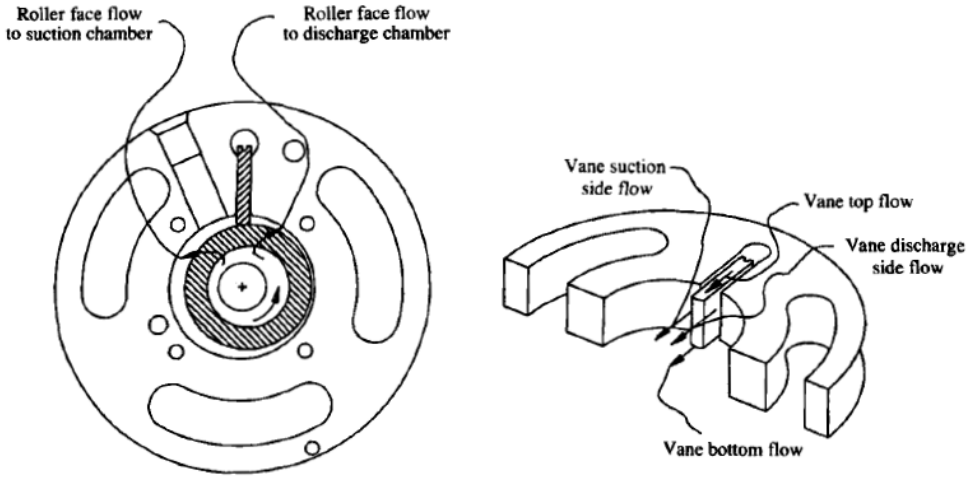

Figure 2.11: Oil flow paths inside the rolling piston compressor taken from [Padhy, 1994].

The oil flows into the compressor through six leakage paths located at the top and bottom of the roller and between the vane and the compressor housing. These paths are indicated in figure 2.11. The flow is driven by the pressure difference between the pressure outside and inside of the compressor chambers and the rotational forces exerted on the oil due to the rotation of the crankshaft and roller. Due to the high pressure difference inside the compressor compared to the rotational forces, most of the driving force comes from the pressure difference.

2.3.4. COMPRESSION POWER

The compression power is needed to estimate how much power the compressor needs to compress the fluid during operation. Because the compression is presumed to be isentropic, the compression power can be calculated with equation 2.21 from [Moran et al., 2012]. While the values for the enthalpy and entropy were extracted from [NIST Standard Reference Database, 2010].

$$\dot{W}_{comp} = \dot{m}\,(H_2 - H_1) \Rightarrow S_1 = S_2 \tag{2.21}$$

2.3.5. COMPRESSOR LOSSES

Besides the heat production due to the compression of the gaseous fluid, the compressor is also heated due to the mechanical losses inside the system. For the losses inside the system a distinction is made between the friction losses inside the compressor and the losses of the DC motor.

FRICTION LOSSES

The losses due to friction are estimated using the formulas given in [Ooi, 2005]. In [Ooi, 2005] six different interfaces in which friction occurs are identified, being:

- Eccentric shaft vs Roller.
- Roller vs Top & bottom flanges.
- Eccentric shaft vs Top & bottom flanges.
- Vane vs Roller.
- Vane vs Vane slot.
- Eccentric shaft vs Bearings.

For the calculations in [Ooi, 2005] the roller rotational velocity was calculated as was done by [Pandeya and Soedel, 1978] and the vane forces were calculated accoring to [Yanagisawa et al., 1982].

MOTOR LOSSES

To calculate the motor losses of the brushless DC motor which operates at high RPM's, [Boukais and Zeroug, 2004] showed that the brushless DC motors at high RPM's have an efficiency between 77-80%. The operational range at which the DC motor of the Purswave compressor can operate is around the range where the efficiency was closer to

80%. Therefore, the motor efficiency for the purswave DC motor was estimated to be $\eta_{DC} = 80\%$. To calculate the total power used by the compressor and power loss due to DC motor losses equation 2.22 is used.

$$W_{tot} = \frac{W_{comp} + Q_{fric}}{\eta_{DC}} \Rightarrow Q_{DC} = W_{tot} - \left(W_{comp} + Q_{fric}\right) \tag{2.22}$$

Here:

- W_{tot} is the total power usage of the compressor.
- W_{comp} is the compression power needed to compress the fluid isentropically.
- Q_{fric} is the total heat production due to friction.
- Q_{DC} is the heat production due to losses of the DC motor.

2.3.6. HEAT CONDUCTION THROUGH COMPRESSOR CASING

The heat transfer from the inside of the compressor casing to the outside is assumed to be a 2D steady state conduction across a cylindrical surface. Since the fluid on top of the compressor housing and the oil around and below it do not conduct heat very well, the assumption was made that they insulate the compressor. Using this assumption the thermal resistances inside the compressor can be calculated using equation 2.23 from [Mills, 2014].

$$R_x = \frac{ln\left(\frac{r_2}{r_1}\right)}{2\pi k_x L_h} \tag{2.23}$$

- R_x = the thermal resistance for each substance.
- r_1 = the inside diameter of the cylinder.
- r_2 = the outside diameter of the cylinder.
- k_x = the thermal conductivity of the substance.
- L_h = the height of the compressor at which the heat transfer is occurring.

To simplify the calculations, the empty areas around the steel of the compressor housing visible in the blue striped areas in figure 2.10 are assumed to be filled up with steel. The thermal resistances and other relevant values for each substance are given in table 2.5.

2.3.7. HEAT EXCHANGER

To improve the heat exchange from the compressor to its surroundings a heat exchanger can be used. First different concepts for the heat exchanger are evaluated and afterwards one concept is further researched and added to the compressor model.

Substance	R_x [K/W]	k_x [W/mK]	r_1 [mm]	r_2 [mm]	L_h [mm]
Aluminium	0.0143	202	50	70	15.0
Steel casing	0.138	58	23.5	50	15.0
Steel caps	0.536	58	4.75	23.55	8.2
Oil	0.0693	0.13	23.53	23.55	15.0

Table 2.5: The relevant measurements for the calculation of the thermal resistances inside the compressor casing. Where the values for the thermal conductivity of steel and aluminum are taken from [Sinnott and Towler, 2013]

HEAT EXCHANGER CONCEPTS

To actively cool the compressor, three concepts were devised and evaluated.

- Active cooling of the oil.
- Active cooling of the compressor casing with a service fluid.
- Active cooling by forced convection of air over the casing.

Oil cooling This concept works by pumping the oil in the casing out of the casing with a small pump and then directing it through several finned tube heat exchangers to cool the oil. Afterwards, the cooled oil is directed back into the compressor casing. The force of the flow with cool oil will induce better mixing inside the oil sump, making the oil sump have a constant temperature. This way the compressor housing will be submerged in a bath of cool oil and will be able to release it's heat better to the oil.
The downside of this concept is that the small pump which induces the flow must be able to withstand a pressure of 50 [bar]. This would mean that the pump would become quite expensive. Also the heat transfer coefficient of the oil is poor. This would result in the need of a very long finned tube heat exchanger which would again be expensive.

Service fluid cooling This concept has the same finned tube heat exchanger but the difference is that the heat exchanger does not carry the high pressure oil, but a service fluid. This service fluid is kept separate from the oil inside the casing. The service fluid would be pumped through the wall of the compressor casing and thereby cooling the casing. The compressor housing can lose its heat through the connections between the housing and the casing. If the heat transfer through the connections is not sufficient, the contact area between the casing and the housing can be increased by filling in the empty spaces between the two indicated with blue in figure 2.10.
This concept is easier to implement since the service fluid does not need to be at high pressures. Because of this, the pump can be cheaper. The downside of this concept is that, because the fluid needs to loose its energy to the ambient air and needs to subtract heat from the casing, two temperature differences need to be present. This reduces the efficiency of the cooling. This would probably result in a big heat exchanger.

Air cooling This concept tries to cool the compressor casing directly, by forcing ambient air directly over the compressor casing with a fan. The outside surface area of the

compressor can also be increased by adding fins to the compressor casing which will improve the heat transfer. The downside of this concept is that the fins would need to be connected very precisely to ensure no air pockets are present in between the fins and the casing. These air pockets would serve as insulators inside the system, which would deter the heat transfer. Another downside of the air cooling concept is that there is a finite amount of heat transfer area available because the compressor has a finite size. This results in limited heat transfer from the compressor.

Chosen concept After evaluating the possible concepts for the heat exchanger, the decision was made to go with the "Air cooling" concept where the outside of the compressor casing is directly cooled with forced convection of ambient air by a fan. The decision was made because it was the cheapest solution and the option that was easiest to implement since only a fan is needed together with fins on the outside of the compressor. Also the heat production of the compressor was assumed not to be too high which ruled out the need for a big heat exchanger surface area.

FIN DESIGN

For the fin design generally two options are used to increase the area of a tube which is roughly the shape of the modular compressor. The fins are either attached radially onto the tube as depicted in figure 2.12 or attached in the longitudinal direction as shown in figure 2.13.

Figure 2.12: Radial finned heat exchanger taken from [Guanyu Tube, 2021]

Figure 2.13: Longitudinal finned heat exchanger taken from [Ningbo Longxuan Aluminium Co., Ltd., 2021]

For this compressor the decision was made to attach the fins radially because that way it is easier to ensure that the fins have perfect contact with the compressor and thereby increasing the effectiveness of the fins. The fins will be aluminum U-profiles visible in figure 2.14. For the U-profile 2 different shapes are ordered because the compressor casing has a smaller radius where the compressor housing is located. Therefore the fins need to be longer at those locations. The dimension of the fins are given in table 2.6.

Side [mm]	a	b	c
Long fins	20	40	2
Short fins	20	20	2

Table 2.6: Measurements of the long and short fins used for the compressor casing. Which letter corresponds to which side is depicted in figure 2.14.

To ensure good connection between the fins and the compressor housing, the surface of the compressor housing on which the fins are mounted is first milled to ensure a flat surface. The U-profiles are fitted at intervals of 45° around the compressor, as depicted in figure 2.15. The air flow from the fan will be directed from the bottom to the top of the compressor. In that way, the flow can move through the spaces in between the fins. Also, in this way the natural convection of the compressor casing will induce an air flow in the same direction. This improves the heat transfer of the air due to the higher velocity with which the air flows over the compressor.

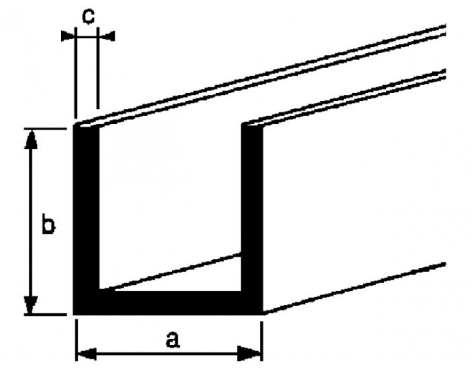

Figure 2.14: Illustration of the U-profile taken from [GYZS, 2021].

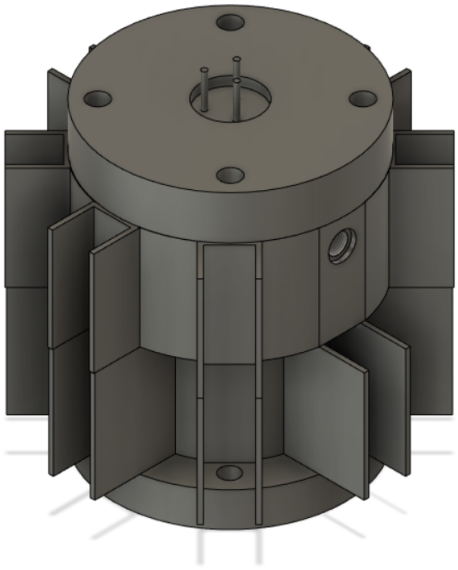

Figure 2.15: Conceptual design of finned compressor casing.

FIN HEAT TRANSFER CALCULATIONS

To simplify the estimation of the heat transfer coefficient of the heat exchanger, all the longitudinal gaps are assumed to be of the same size. Also, the assumption is made that the entire mass flow created by the fan will flow through these holes and will not leak out of these holes radially. These simplifications make the calculations easier and give a

rough estimation on the heat transfer of the heat exchanger.
To calculate the heat transfer coefficient, the Nusselt number and the Reynolds number need to be calculated. After calculating the heat transfer coefficient, the efficiency of the fins can also be estimated.

Reynolds number The Reynolds number (Re_{air} is calculated for a rectangular channel. To calculate the hydraulic diameter (D_h) for a rectangular channel the left part of equation 2.24 can be used according to [Engineering ToolBox, 2003] & [Ratzlaff, 2018]. Afterwards the Reynold number can be calculated using the right part of equation 2.24.

$$D_h = \frac{2L_w L_{he}}{L_w + L_{he}} \Rightarrow Re_{air} = \frac{v_{air} D_h}{\nu_{air}} \tag{2.24}$$

Here:

- $L_w = 20$ [mm] is the width of the channel.
- $L_{he} = 20$ [mm] is the height of the channel.
- $v_{air} = 3.76$ [m/s] is the velocity of the air inside the channel.
- $\nu_{air} = 1.54 * 10^{-5}$ $[m^2/s]$ is the kinematic viscosity of the air calculated using [NIST Standard Reference Database, 2010].

Nusselt number After calculating the Reynolds number the Nusselt number can be calculated with the formula corresponding to the found Reynolds number, which is equation 2.25 according to [Mills, 2014]. The friction factor (f_{Nu}) used in this formula can be calculated using equation 2.26. The Prandtl number (Pr_{air}) of the air is again extracted from [NIST Standard Reference Database, 2010] just like in chapter 2.2.3.

$$Nu_{air} = \frac{\frac{f_{Nu}}{8}(Re_{air} - 1000)\, Pr_{air}}{1 + 12.7\frac{f_{Nu}}{8}\left(Pr_{air}^{\frac{2}{3}} - 1\right)} \tag{2.25}$$

$$f_{Nu} = (0.790 \ln(Re_{air}) - 1.64)^{-2} \tag{2.26}$$

Heat transfer coefficient of the air flow Finally, the heat transfer coefficient can be calculated using the rewritten formula for the Nusselt number just like it was done in equation 2.7. The thermal conductivity (k_{air}) is again calculated using [NIST Standard Reference Database, 2010].

$$h_{air} = \frac{2Nu_{air} k_{air}}{D_h} \tag{2.27}$$

Fin efficiency To be able to calculate the heat transferred from the fins, the temperature profile across the length of the fins needs to be calculated. This is important because if there is a big temperature difference between the base of the fin and the tip of the fin, there will be less heat transfer on the tip than on the base of the fin. To calculate the fin efficiency, first the fin parameter is calculated using equation 2.28 and afterwards the temperature along the fin is calculated using equation 2.29; both are taken from [Mills, 2014]. If the temperature of the tip fin is close to the temperature of the base of the fin, the efficiency of the fin is very high. With a high fin efficiency, the assumption that the heat transfer to the air is equal for every location along the fin, can be used.

$$P_f = 2t_f + 2L_h, comp \Rightarrow A_f = t_f L_{h,comp} \Rightarrow \beta = \left(\frac{h_{air} P_f}{k_{alu} A_f}\right)^{0.5} \tag{2.28}$$

Here:

- P_f is the circumference of the fin.
- t_f is the thickness of the fin.
- $L_{h,comp}$ is the length along the casing to which the fin is mounted.
- A_f is the surface area of the fin.
- β is the dimensionless fin parameter
- k_{alu} = 202 [W/mK] is the thermal conductivity of aluminum according to [Sinnott and Towler, 2013].

$$\frac{T - T_{air}}{T_b - T_{air}} = \frac{cosh\,\beta\left(L_f - x\right)}{cosh\,\beta L} \tag{2.29}$$

Here:

- T is the temperature of the fin at location x along the fin.
- $T_a$ir is the temperature of the ambient air.
- T_b is the temperature at the base of the fin.
- L_f is the length of the fin.
- x is the location along the fin where x = 0 is the base of the fin and x = L_f is the tip of the fin.

3

METHOD

In chapter 2.2 a rough estimation was made on what is happening inside the compressor. Using this rough estimation the decision was made to further research the active cooling of the compressor using the concept of "Cooling through the compressor housing".

The concept of cooling through the compressor housing was put to the test using the method described in this chapter. First, a computational model was made using the theory described in chapter 2.3. This is described in section 3.1. Afterwards, the calculations and results from the computational model are verified by doing experimentation into the important calculated values of the model. How the experiments were prepared and executed is described in 3.2.

3.1. COMPUTATIONAL MODEL

The computational model is used to more accurately predict whether the concept for active cooling "Cooling through the compressor housing" from chapter 2.2.3 is still viable. For this the theory and formulas previously described in chapter 2.3 are implemented into a script. The model has the goal to be able to calculate what is happening inside the compressor. To get an idea of what is occurring inside the compressor, three main things want to be known:

1. Mass flow induced by compressor
2. Power usage of the compressor
3. Steady state temperatures of compressor at different locations

A simplified depiction of the way the model is calculated is depicted in figure 3.1. The script starts by defining the compressor parameters like the measurements of the roller. After defining the parameters, the compression chamber volume can be calculated using equation 2.16. This is done with iterative steps for each step the roller rotates.

After each compressor chamber volume is calculated, the pressure inside the chamber can be calculated using equation 2.13. After the pressure is calculated, the leakage

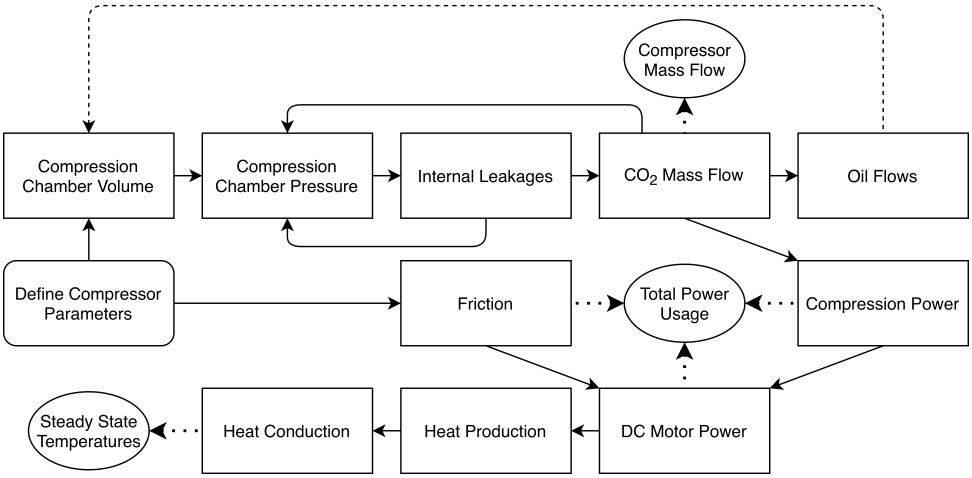

Figure 3.1: The stepwise process in which the computational model is constructed. Full lines indicate a direct correlation, Dashed lines indicate a direct correlation that is not taken into account in this model and dotted lines are to indicate where the important calculated values can be extracted from the model.

can be estimated using equation 2.17. Using this leakage rate, the pressure of the compression chamber can be corrected with equation 2.19. If the pressure inside the compression chamber is higher than the pressure in the compressor casing on the other side of the valve, then mass is transferred to the casing until the pressure inside the compression chamber is again equal to the pressure in the casing. This can be calculated using equation 2.20.

After these values are calculated for every position of the roller, the total mass that flowed out of the compressor can be determined together with the power needed to compress the fluid. The power is calculated for every step using equation 2.21. The mass flow in this formula is calculated for every step, by dividing the mass that is left inside the compression chamber with the time step needed to rotate the roller one step. Meanwhile. for every roller position the pressure is also known. This is then used to calculate the oil flows inside the compressor using the formulas provided by [Padhy, 1994].

In this model, the assumption was made that the oil flowing inside the compressor would have such a low volume flow that it would not influence the dead volume of the compressor during compression. To simplify the calculations, the assumption was made that there was no oil present inside the system. This is however not the case in reality. Therefore this correlation is only depicted with a dashed line to indicate that there might be a need to implement this in the future. However, it is not done in this model.

The friction losses inside the compressor can be calculated using the formulas from [Ooi, 2005]. Afterwards the DC motor losses can be calculated using equation 2.22, because both the friction losses and power needed for compression are known.

The next thing that is calculated is the temperature of the fluid after adiabatic compression using equation 2.1. Together with the losses inside the system, the amount of

heat that is produced is then known.

Afterwards, the heat conduction through the compressor casing is calculated as mentioned in chapter 2.3.6, together with the convection of heat at the fins as described in 2.3.7.

Using the heat production and conduction of the compressor, a thermal resistance scheme can be set up as depicted in figure 3.2. After solving the system, all temperatures in the figure can be calculated to gain a first idea of the steady state temperatures of the compressor. Important to note is that the assumption is made that no radiative heat transfer is occurring. This assumption was mainly made because the emissivity of the alluminum casing and the steel fan duct are very high. This causes the compressor to be insulated in respect to its radiative heat transfer.

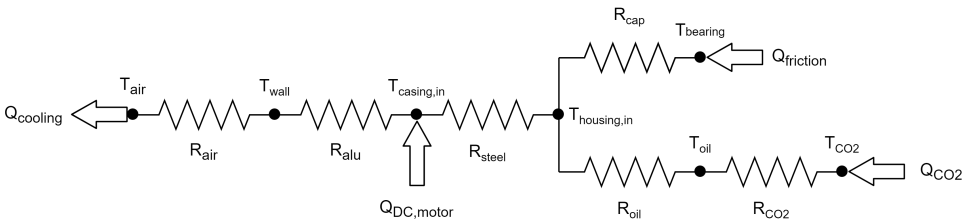

Figure 3.2: Thermal Resistance Scheme used to calculate the steady state temperatures of the compressor. The arrows indicate at what locations the heat is added to the system while the zigzag lines indicate the thermal resistances of the compressor

3.2. EXPERIMENTATION

To validate the results of the computational model, experiments were conducted. These experiments will be further explained in this section. In the earlier stages of this thesis, experimentation was conducted on the oil flow inside the compressor, which will be explained further in chapter 3.2.1. At the end of the thesis, the steady state values of the compressor were assessed. This will be further elaborated in chapter 3.2.2.

3.2.1. OIL FLOW EXPERIMENTATION

The oil flow experiment was build and tested to validate the results from the oil flow calculations from [Padhy, 1994]. For the oil flow to be measured, the holes on the outside of the compressor housing were sealed of to prevent the oil from flowing back which is visible in figure 3.3. To prevent a pressure difference between the top of the compressor casing and the bottom of the compressor casing, a loop was added to the casing as depicted in figure 3.4. In this way, the pressure would be evenly distributed but oil would not be able to flow back. Afterwards, the bottom chamber was filled with oil until no air remained in the bottom chamber. This was done to prevent compression of the air pockets. The oil level could be read out through the transparent PFA tube in the outside loop, visible in figure 3.4. When the compressor was turned on, the drop in oil level inside the tube should give an estimate of how much oil the compressor is using during operation because the compressor pumps oil from the bottom to the top chamber.

After multiple experiments were conducted, this experiment was aborted because the oil level was oscillating vigorously. Because of this, the oil level could not be properly read out over time. Therefore, no conclusion could be made from the experiment.

Figure 3.3: Sealing applied to inside of the compressor casing to prevent flow back into oil reservoir.

Figure 3.4: Loop outside of compressor casing to let both the top and bottom chamber equalize in pressure without enabling oil to flow between both chambers.

3.2.2. STEADY STATE EXPERIMENTATION

To examine the outputs of the computational model and to asses the effectiveness of the active cooling of the compressor, steady state experimentation was conducted. Here, the compressor was turned on until all temperatures inside the compressor did not increase any further than 1 degree Celsius per 1000 seconds. This chapter does not go into detail on the accuracy of the measurements. The accuracy of the measurements is explained in depth in appendix A.

EXPERIMENTAL SETUP

The compressor was attached to a wooden board with 100 [mm] clamps. Afterwards, the compressor was encased in the fan duct as is visible in figure 3.6. The holes on the sides of the fan duct were closed off with tape to ensure the flow induced by the fan could only be sucked in through the bottom of the fan duct. Afterwards, the fan duct was insulated to make sure all the heat that was generated by the compressor would leave through the top of the fan duct and the outlet of the compressor. The fan was placed on top afterwards. This part of the setup is visible on the left side of the wooden board in figure 3.5. On the left of the fan duct in figure 3.5, the inlet of the compressor is visible. On the inlet of the compressor, a check valve was installed to prevent backflow of oil. The outlet of the compressor was attached to a pressure tank which has a copper mesh inside it to

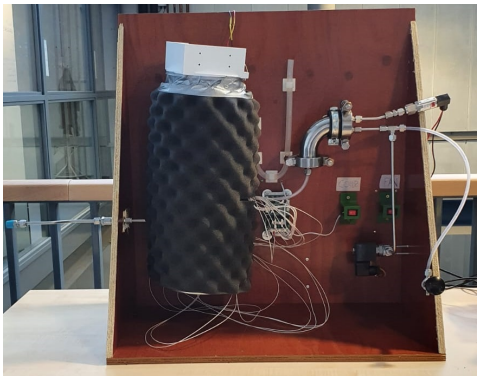

Figure 3.5: The finished assembly of the compressor setup.

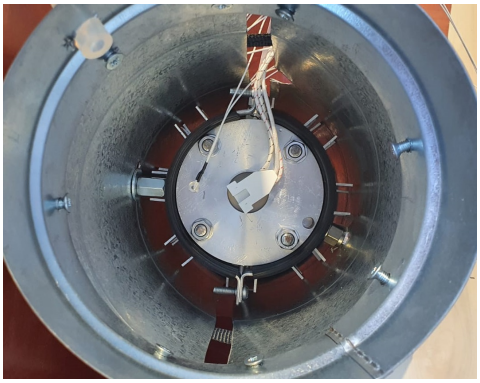

Figure 3.6: The compressor with fins assembled inside the fan duct but without insulation.

prevent oil from being discharged from the system. The pressure tank had a pressure sensor installed on the top right connector of this tank, while the bottom connector on the right of the pressure tank was connected to a solenoid valve to electronically release pressure from the system and to a needle valve to manually discharge the pressure.

TEMPERATURES

Multiple negative temperature coefficients (NTC's) were placed throughout the compressor to determine the temperature at different locations of the compressor and to asses whether the compressor had reached steady state yet. The location in which these sensors were place are shown in figure 3.7.

1. The first NTC is placed right above the outlet of the compression chamber. This was done because the temperature of the compressed gas is presumed to be the highest temperature inside the system. The NTC was placed right above the valve to make sure the temperature is close to the temperature which it was during compression.

2. The temperature at this location is measured to get an idea of how much heat is being produced by the coil. Using this temperature, an assumption can be made whether the motor efficiency of 80% is close to the reality of the situation.

3. This NTC is placed in between the fins and the outside wall of the compressor. This temperature can be used to asses the effectiveness of the fins and whether the heat is evenly distributed over the entire aluminum casing.

4. After the fluid is discharged from the compressor, the temperature is presumed to cool down because the volume above the motor is filled with gas that is exchanging heat to the compressor casing. Therefore another sensor was place above the coil to measure the temperature of the bigger volume.

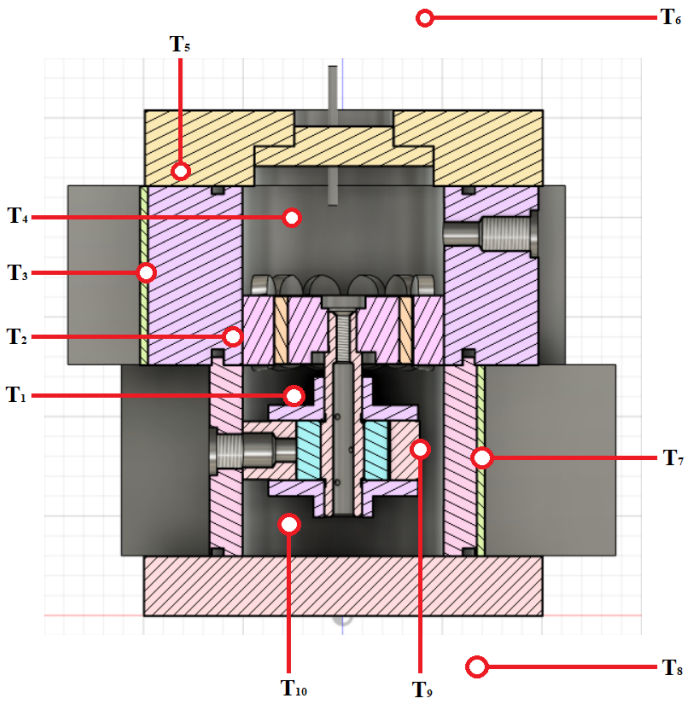

Figure 3.7: Cross section of the compressor with the location of the NTC's highlighted.

5. The sensor in the top cap shows whether the temperature is evenly distributed over the compressor casing and if temperature can be properly conducted from one casing part to the other.
6. Since there is an updraft along the compressor, this sensor can measure how much the air has heated up after being passed along the compressor.
7. Here, the temperature of the wall of the lower compressor casing is measured for the same purpose as T_3.
8. Below the compressor, the ambient temperature is measured. This can be used for the inlet conditions of either the compressor or the fan duct.
9. The temperature in the middle of the steel compressor housing is measured here to see how the temperature gradient from the outside towards the inside develops.
10. The tenth and final NTC measures the temperature of the oil reservoir to see at what temperature the oil is sucked into the compressor housing.

MASS FLOW OF COMPRESSOR

The pressure inside the pressure vessel is regulated using a pressure sensor and a solenoid valve. Once the pressure goes above the desired pressure, the solenoid valve opens and

releases the pressure in puffs until the pressure is again below the desired pressure. By switching off and on, the pressure increase can be determined multiple times in one measurement. This pressure increase inside the pressure vessel - just before the pressure is released by the solenoid valve - can be used to determine the mass flow of the system. First the density of the fluid was extracted from [NIST Standard Reference Database, 2010] using the pressure and temperature of the vessel before and after the measured time step. Using the density, the amount of mass that was added to the system in that time step can be calculated using equation 3.1.

$$\dot{m}_{comp} = \frac{(\rho_2 - \rho_1) V_{vessel}}{(t_2 - t_1)} \tag{3.1}$$

- ρ_1 = the density inside the vessel at the beginning of the timestep.
- ρ_2 = the density inside the vessel after the timestep.
- V_{vessel} = the total volume in which the fluid sits, which includes the pressure tank compressor casing and tubing.
- t_1 = the time at the beginning of the timestep.
- t_2 = the time after the timestep.

POWER USAGE

The power usage is determined by measuring the current going to the compressor electrical board. This was done because this is DC current, which is much easier to read out with the electronics available than the AC current; which flows through the three phase power wires going from the electronic board to the compressor. By multiplying the current with the voltage provided by the power supply, the total power usage of the compressor could be calculated.

FRICTION LOSSES

The friction losses were calculated by multiplying the total power usage with the DC motor efficiency and then subtracting the isentropic work of the compressor, which is calculated with the mass flow of the system as shown in equation 3.2.

$$Q_{fric} = \eta_{DC} W_{tot} - \dot{m}_{comp} (H_2 - H_1) = \eta_{DC} W_{tot} - W_{comp} \tag{3.2}$$

COOLING POWER

During the experiment, an attempt was made to asses how much the flow of air cools down the compressor. The outside of the fan duct was insulated to ensure as little heat exchange as possible. Then using the inlet and outlet temperatures of the fan duct together with the volumetric flow of the air in the duct, the cooling power can be estimated. The volumetric flow is estimated by measuring the pressure drop over the fan. The pressure drop can be measured with a water seal which is depicted in figure 3.9. By looking at the difference in height of the water level in the water seal, the fan performance can be read out from the fan performance curve, which was provided by the company produced the fans, as depicted in figure 3.8.

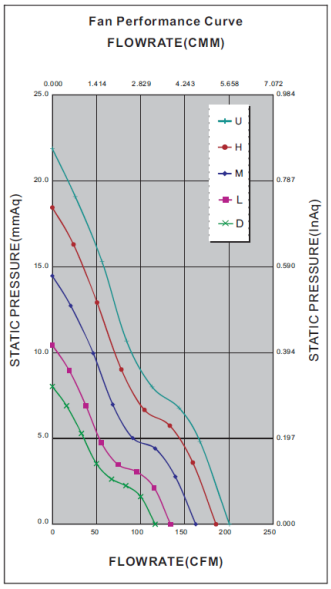

Figure 3.8: Cooling fan performance curve. With the flowrate on the x axis and the water level difference on the y axis. Here line H corresponds to the fan that was used

Figure 3.9: Water seal in place to estimate pressure drop over the cooling fan.

FIN EFFICIENCY

To validate if the fin efficiency is calculated correctly, the temperature along the fins must be measured. This is however very hard to measure correctly with NTC's, because the sensors cannot be properly embedded into the fins. Therefore the decision was made to measure the temperature glide with a infrared camera. However, because the casing is made of aluminum which has a high emissivity coefficient, the temperature is hard to measure with an infrared camera. Therefore, the two fins that are located on the front of the compressor were painted matt black to decrease the emissivity coefficient. Afterwards, the compressor was turned up to 6000 [RPM] and to 7.1 [bar] to get the maximum temperature at the wall of the casing. Then the fin was photographed while the fan was on and while the fan was off. The results of this experiment are displayed in chapter 4.1.5.

METHOD OF EXPERIMENTATION

To asses the impact of the changes made to the compressor, four different configurations were tested at 2000 to 6000 [RPM] with intervals of 1000 [RPM]. All these tests were run for a 2 stage and a 3 stage compression system. However, only on the first stage of these systems experiments were conducted, since that was the only stage where the data could be produced correctly. The higher stages were still under construction during this thesis. However, because the temperature increase due to compression is mostly correlated with the pressure ratio, a good estimation of the performance can be made by only

testing the first stages. The 3 stage system would compress from ambient pressure to 3.7 [bar], while the 2 stage system would compress from ambient pressure to 7.1 [bar].

4

Results and Discussion

In this chapter, the results from the computational model and the experimentation are first compared in section 4.1. Afterwards, the results for the comparative experiments regarding the different cooling settings are shown in section 4.2. Next, the results for the experimentation on the dependence of the mass flow and the power usage on the temperature of the oil reservoir are presented in section 4.3. Finally, the model was changed to handle carbon dioxide instead of ambient air. The results of this experiment are shown in section 4.4.The results are discussed after each figure to interpret the meaning of the results.

4.1. Model vs. Experimentation

To check whether the computational model is correct, experimentation was done on the following 5 parameters: casing temperature distribution; steady state temperatures; mass flow; power usage; and fin efficiency. These are each explained separately in this section.

4.1.1. Casing temperature distribution

In chapter 3.2.2 it was mentioned that the temperature difference between different locations of the compressor casing were measured to asses the conductivity of the aluminum casing. The model predicted that the temperature difference would be very low, about 2 [K]. The experimentation showed similar temperature differences over the casing for all the different cooling settings. Therefore, it can be stated that the aluminium casing has a uniform temperature distribution. However, due to this similarity of the temperatures over the casing, the NTC near the motor coil could not give values which were accurate enough to draw conclusions regarding the motor efficiencies.

4.1.2. Temperatures

To asses whether the conduction scheme depicted in figure 3.2 and the thermal conductance's calculated by the model are correct, the temperature differences for the model

and experimentation are depicted in figure 4.1.

DISCHARGE TO STEEL

From the figures, it is clearly visible that the modelled temperature difference between the discharge of the compressor and the steel casing is very different from the experimental values for both the 2 and 3 stage compressors. This could be caused by multiple factors. First of all, the heat transfer coefficient of the carbon dioxide might be underestimated by the model. An other explanation would be that the assumption made in chapter 2.2.3, that there is no atomization of the lubricant, was false resulting in an additional source of cooling for the compressed gas. Finally, the measurements might differ from the model because of the location of the measurement, which was just outside of the valve. However, the compressed gas might already have cooled down before flowing over the NTC, or oil on top of the compressor might be disturbing the measurements of the NTC.

STEEL TO WALL

The temperature difference between the steel housing and the wall of the compressor is much higher for the experimental values then for the modelled values. This is most likely because of the assumption of 2D heat transfer and because the steel casing was assumed to have no holes as depicted in figure 2.10. This would mean that thermal resistance is greater due to the gaps of oil and that there is more heat transfer from the top and the bottom of the compressor to the oil reservoir surrounding the compressor. The heat transfer to the oil might be increased due to the flow of oil around the compressor which might be induced by the rotating compressor shaft.

WALL TO AIR

Finally, the heat transfer of the compressor wall to the flow of ambient air seems to be predicting the temperature difference quite accurately. This can be stated because even though the temperature difference seems to have been underestimated, the experimental power usage of the compressor is around 2 times as big as the modelled power usage, which is further explained in section 4.1.4. This would mean that if the power usage was the amount with which the model predicted, the values would align better.

MAXIMUM TEMPERATURE

The discharge temperature is also calculated and measured, which is depicted in figure 4.2. With the inlet and discharge temperatures, the polytropic coefficient of compression can also be calculated which is shown in figure 4.3. Preferably, the discharge temperature stays below 100 $[^oC]$ to prevent thermal degradation of the lubrication. While the model predicted that the discharge temperatures would go up to 100 $[^oC]$ or even above it for the 2 stage version, the experimentation showed otherwise and showed that the compressed fluid is cooled a lot more then modelled. From figure 4.3 it is clear that the compressor seems to run closer to isothermal compression then estimated. What also can be stated is that the model underestimates the heat transfer for the 2 stage system when the compressor is running at lower RPM's. This might be because the friction losses inside the system are actually much higher then modelled, which is further explained in section 4.1.4, or because the mass flow through the system is modelled to be very low at lower RPM's as is further explained in section 4.1.3.

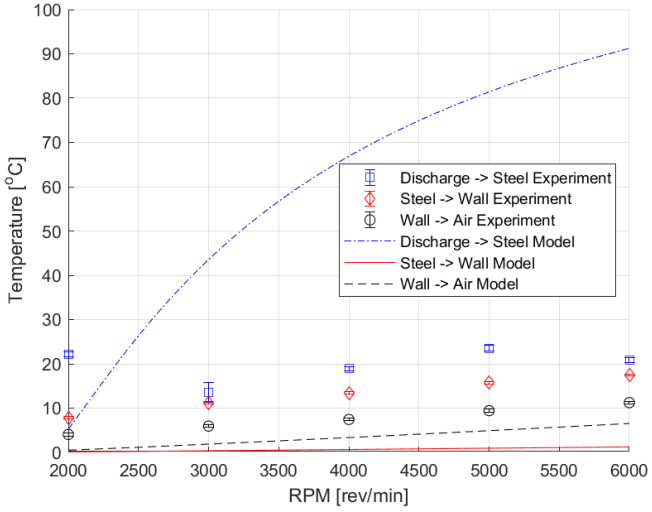

(a) 2 stage

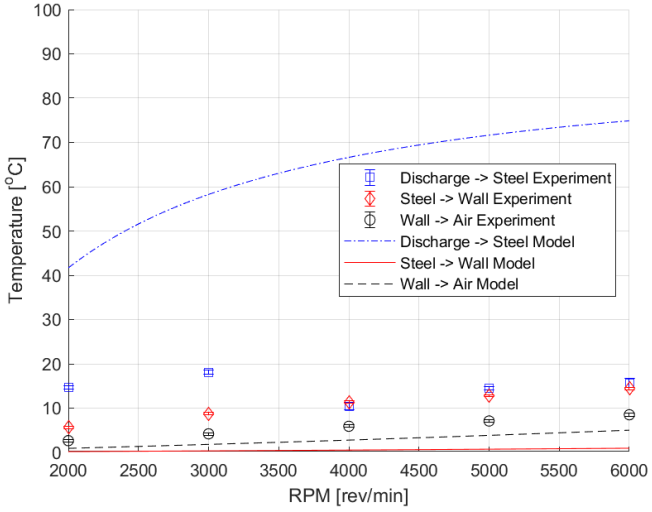

(b) 3 stage

Figure 4.1: Temperature difference between measuring points of the experimentation plotted together with the temperature difference calculated using the computational model. Both plots are depicting the results for the first stage of the system.

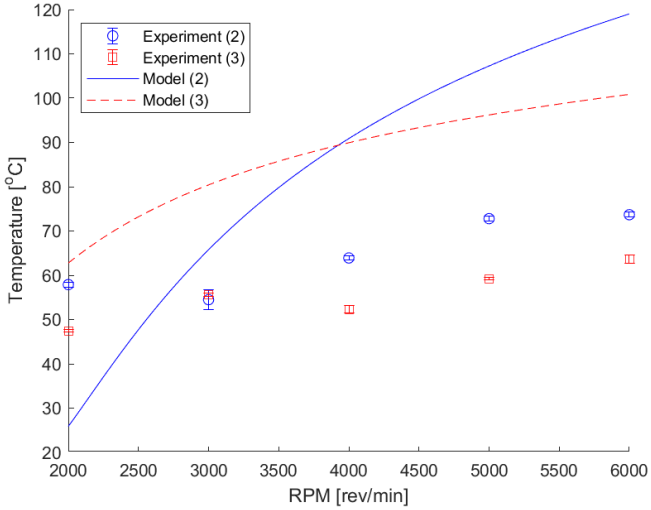

Figure 4.2: The discharge temperature for the 2 and 3 stage compressor for the experimental data and the model results. Here the discharge temperature clearly stay below the desired 100 [°C] for the experimental values

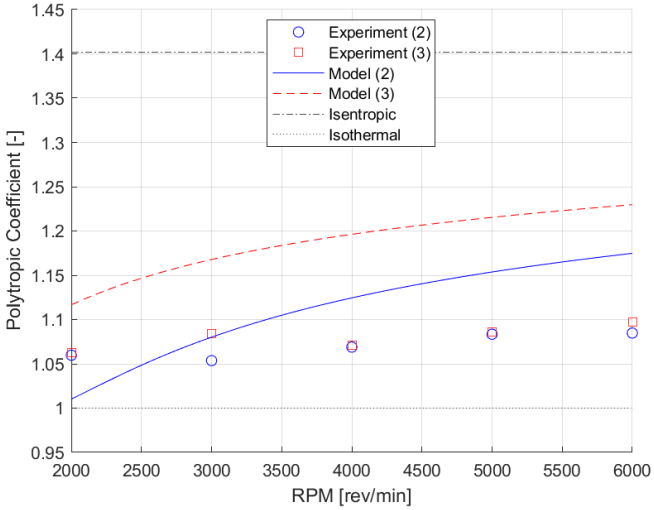

Figure 4.3: Polytropic coefficients for the 2 and 3 stage compressor for the experimental data and the model results. The experimentatal values show that the compression is closer to isothermal than expected.

4.1.3. MASS FLOW

An experiment was conducted on the mass flow of the compressor to see if the desired mass flow stated by the constraints of the system could be reached. The modelled and experimented values are depicted in figure 4.4. From these mass flows, the volumetric efficiency of the compressor can also be calculated which is depicted in figure 4.5.

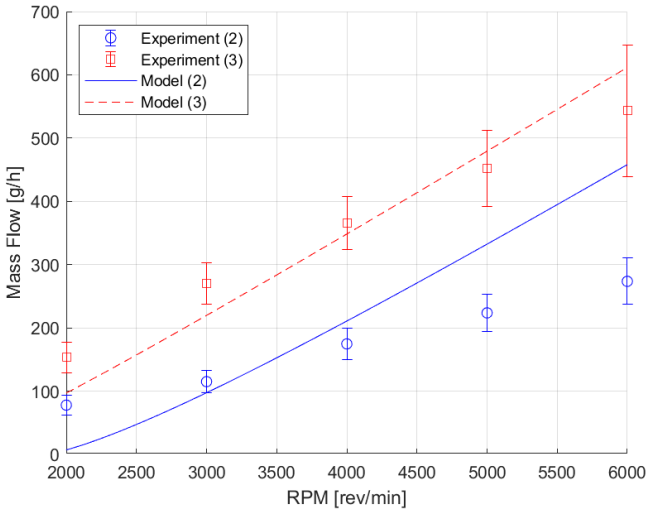

Figure 4.4: The mass flow for the 2 and 3 stage compressor for the experimental data and the model results. The experimental data coincides somewhat with the model however at higher and lower RPM's the model is further off.

Important to note is that the 2 stage system does not reach the desired mass flow of 336.7 [g/h]. The mass flow of the system is predicted quite well. However, the values from the model and the experiment seem to deviate more at the lower and higher RPM's. A cause for this might be that the pressure regulation by the solenoid valve does not account for the rotational speed of the compressor. Therefore, the pressure differences measures are different for each RPM and the pressure at which the solenoid valve opens is different. The graphs depicting this difference are shown in appendix A. Because of this difference, the mass flow might be influenced. A way to fix this problem might be to increase the tank volume. This should decrease the pressure increase in the vessel, which thereby decreases the pressure differences between measuring points. A second cause for the deviation of the values might be the check valve. The check valve was installed in front of the compressor, which showed a pressure drop of 0.111 [bar]. Because of this pressure drop, the compression ratio and the pressure difference of the compressor are increased. This again might reduce the mass flow of the compressor. A final cause for the deviation in the calculation might be that the flow of oil into the compressor is not taken into account. This flow increases the dead volume of the system and thereby decreases the mass flow.

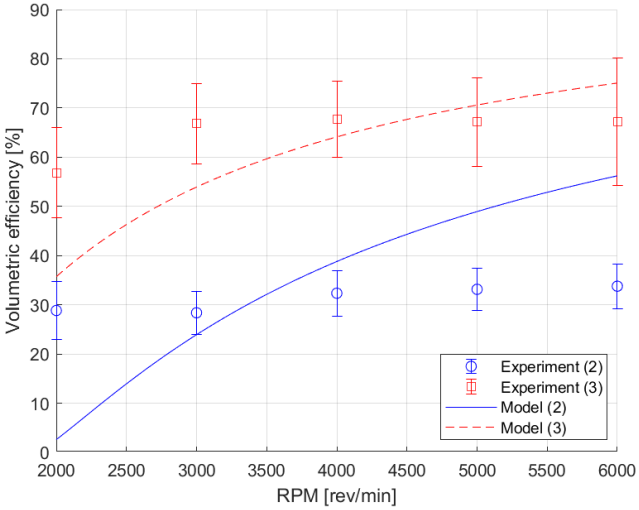

Figure 4.5: The volumetric efficiency for the 2 and 3 stage compressor for the experimental data and the model results. The volumetric efficiency is again modelled well but not for higher and lower RPM's

4.1.4. POWER USAGE

The power usage of the system is important to model and research, because it not only impacts the efficiency of the system but also the amount of heat that is produced by the system. The total power usage of the compressor together with the corresponding compressor efficiencies are depicted in figure 4.6 & 4.7 respectively.

TOTAL POWER USAGES, FRICTION & EFFICIENCY

In these figures it is clear that the power usage of the system is underestimated, which can be explained by looking at figure 4.8. When comparing the power usage with the friction losses it can be stated that the underestimation of the compressor losses is mostly caused by the faulty calculation of the friction losses inside the compressor, since the differences between the modelled and experimental friction losses are roughly the same as the differences between the modelled and experimental total power usage.

COOLING POWER

An attempt was also made to determine how much heat was extracted from the compressor by analysing the temperature difference between the inlet and outlet of the fan duct. The results of this experiment is shown in figure 4.9. However, because the air flow over the compressor was very high, the air did not heat up very much. Because of this the temperature difference was very small and difficult to read out properly with the equipment that was used. A trend is visible in the figure and the cooling power somewhat matches the data from the total power usage of the system in figure 4.6. However, the measurements are not very precise.

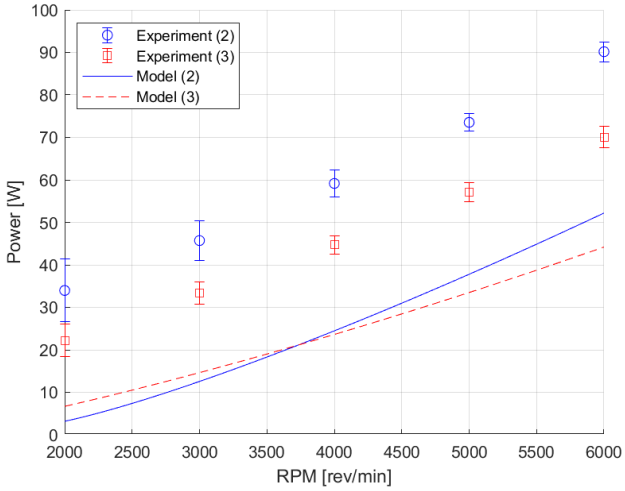

Figure 4.6: The power usage for the 2 and 3 stage compressor for the experimental data and the model results. The offset is most likely due to the faulty friction calculations which is visible in figure 4.8.

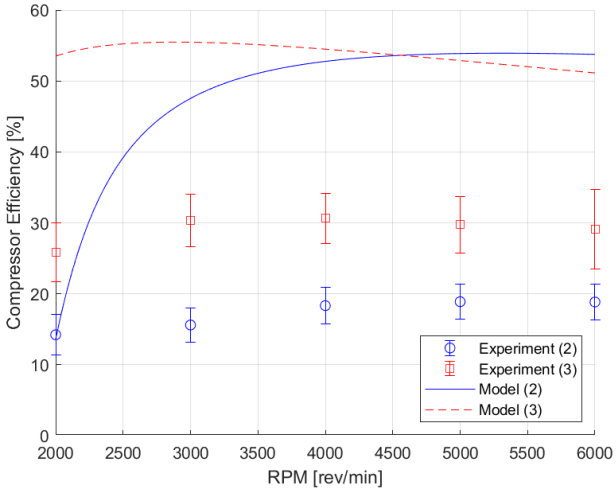

Figure 4.7: The compressor efficiency for the 2 and 3 stage compressor for the experimental data and the model results. The efficiency is underestimated due to the underestimation of the friction as visible in figure 4.8. The reason why the lower RPM's for the 2 stage system is better predicted is because of the very low mass flow of the model which is visible in figure 4.4

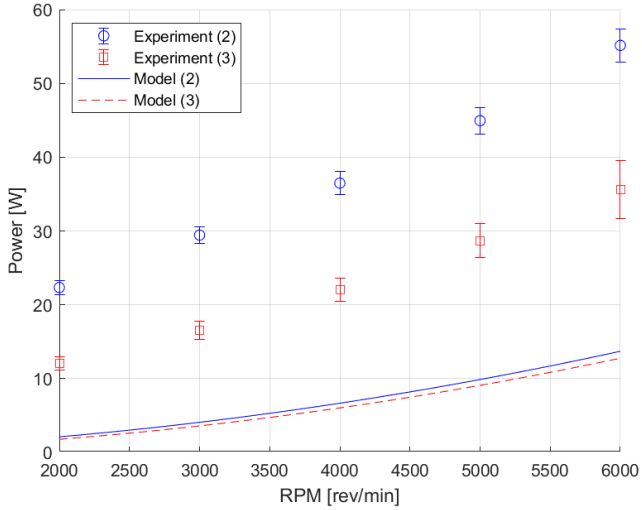

Figure 4.8: The friction losses for the 2 and 3 stage compressor for the experimental data and the model results. The friction forces are underestimated a lot by the model.

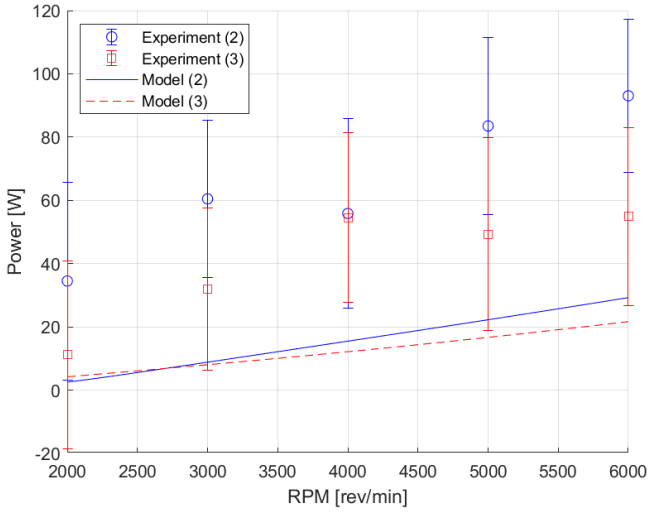

Figure 4.9: The cooling power for the 2 and 3 stage compressor for the experimental data and the model results. The data is however very scattered and therefore not reliable. But a trend is visible.

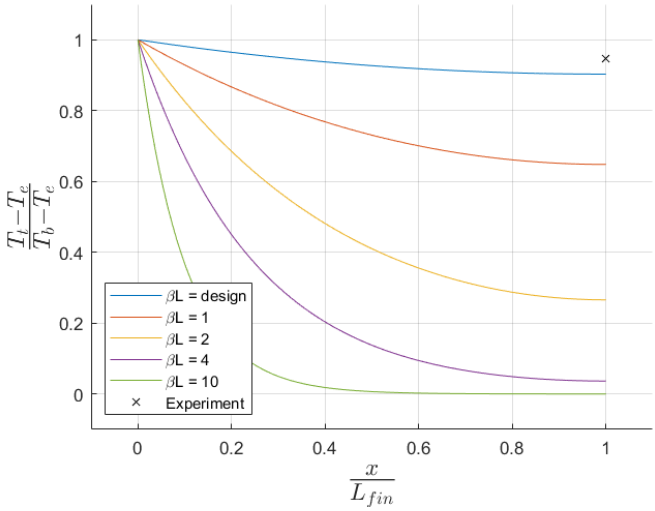

Figure 4.10: Fin temperature distribution as calculated by equation 2.28 together with a single data point taken from the infrared pictures. The model seems to be overestimating the heat transfer. But the fin temperature is higher in reality. Therefore the assumption of constant temperature along the fin is valid.

4.1.5. FIN EFFICIENCY

To asses whether the modelled fin efficiency shown in figure 4.10 was correct, infrared pictures were taken of the compressor during operation. These pictures are depicted in figure 4.11. There seemed to be a smaller temperature drop then expected by the model, resulting in an improved fin efficiency. Therefore, the assumption that the fin has about the same temperature along its length is valid. It is however important to note that this measurement does not precisely measure the tip and base temperature. However, it can give a nice estimation of what is happening on the fin.

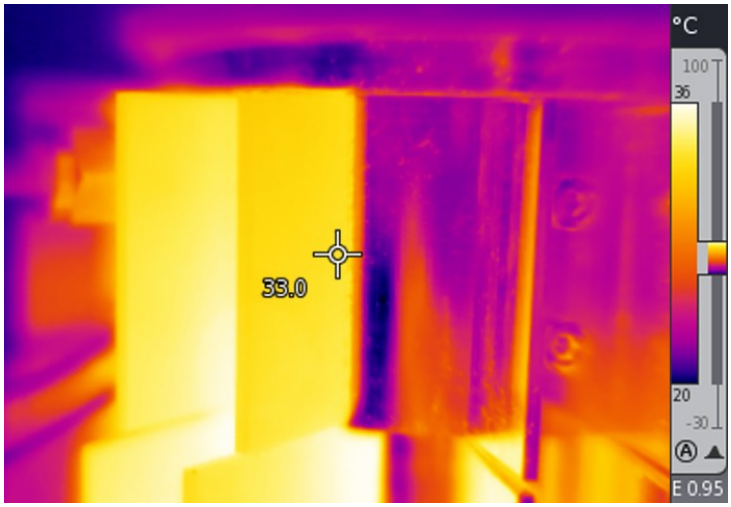

(a) Fin base temperature

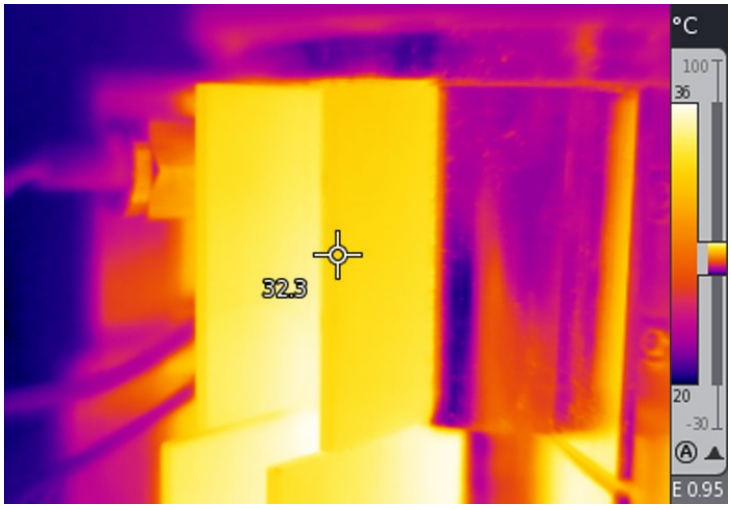

(b) Fin tip temperature

Figure 4.11: Pictures taken with the infra red camera to asses the fin efficiency. The value in the picture indicated the temperature at the centre of the cross in the picture. It is clear from these figures that only the fins that were painted black give a correct reading. The compressor casing is purple in the picture but the sensors over the casing determined that the casing has an uniform temperature. Therefore only the bright yellow part of the figures are correct.

4.2. ACTIVE COOLING COMPARISON

To asses the impact of the applied cooling settings of the fan and the fins, comparative experiments were run with each of the cooling settings, being: "Fan + Fin", "Fin", "Fan" and the "Base" compressor without any cooling additions.

4.2.1. DISCHARGE TEMPERATURES

To show the difference in cooling provided by each setting, the discharge temperatures are plotted besides one another in figure 4.12. From these figures it is clear that the discharge temperature can be kept below 100 [^{o}C] for certain settings but will go above the threshold for the fanless designs. Important to note is that the compressor was ran with ambient air varying between 22 and 26 degrees. However, the system would also need to stay below the threshold of 100 [^{o}C] when operating with an ambient temperature of 40 [^{o}C]. This would mean that the compressed gas would heat up more because the inlet temperature would be higher and that the cooling power of the air around the compressor is decreased due to the higher temperatures. Therefore, the temperature threshold for a valid design is lowered to 80 [^{o}C] at max RPM to make sure the temperature will stay below 100 [^{o}C] in other climates. With this new threshold there are only 3 settings which can cool the compressor adequately, being: "3-stage Fan", "3-stage Fin + Fan" and "2-stage Fin + Fan".

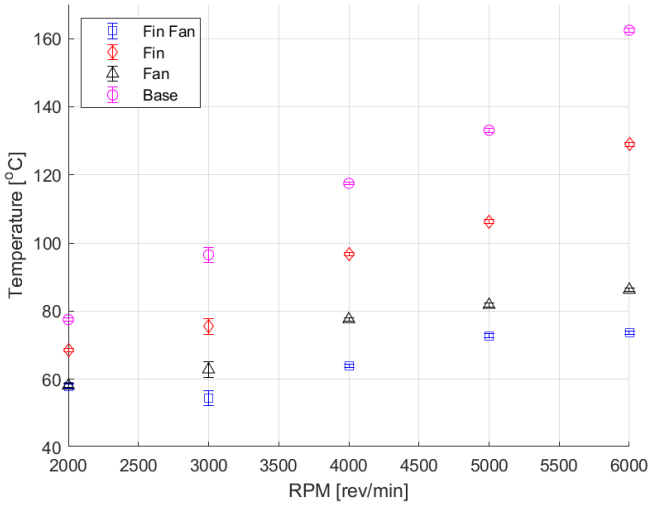

(a) 2 stage

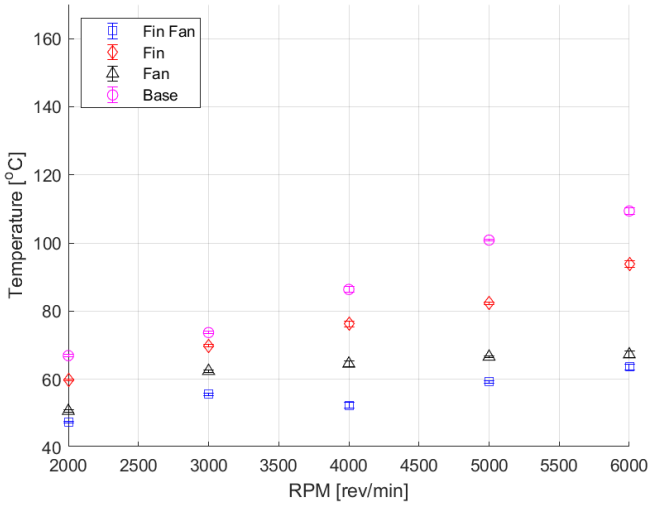

(b) 3 stage

Figure 4.12: Temperature outside of the valve of the compressor for different cooling settings per RPM. The maximum temperature inside the compressor is clearly higher for the 2 stage then the 3 stage. Also the "Fin Fan" cooling setting clearly cools the best. Important to note is that the cooling settings clearly have an impact on keeping the insides of the compressor colder.

4.2.2. HEAT CONDUCTANCE

The heat conductance of each cooling setting is also evaluated to asses their effectiveness. Three conductance paths are evaluated: casing wall to air, casing wall to steel housing and the steel housing to the compressed fluid. Important to note is that the power usage for all the cooling settings are between 80 and 90 [W].

AIR SIDE CONDUCTANCE

The temperature differences between the casing wall and the ambient air are depicted in figure 4.13. Here it is clearly visible that the temperature difference is the lowest for the "Fin + Fan" setting. Because the power usage is somewhat similar for all the cooling settings, the amount of heat conducted from the wall is somewhat similar for all the cooling settings. Therefore, it can be stated that the heat transfer is very good for the "Fin + Fan" setting, whereas the "Fan" setting is a close second place and the temperature difference of the other 2 settings are much poorer. The big differences are off course the higher amount of surface area available for heat transfer in the settings with fins and the improved convective heat transfer of the settings using the fan.

COMPRESSOR CASING & CHAMBER CONDUCTANCE

For the temperature difference between the casing wall and the housing steel the results are shown in figure 4.14. What is interesting to note is that the results are somewhat flipped. Here the settings with a fan have a bigger temperature difference than the settings without the fan. However, because all the settings should have no differences in thermal conduction the only thing that can differ is the amount of heat conducted. This can be caused because more heat is conducted out of the compressed fluid and because the viscosity is decreased due to the increased temperature of the reservoir, which in turn decreases the friction losses of the compressor.

INTERNAL CONDUCTANCE

The temperature difference from the inside of the compressor to the steel housing for all cooling settings are depicted in figure 4.15. From these figures it is very difficult to draw conclusions. The data seems to be quite erratic. To verify the results some duplo's were run for these experiments. However, they did not deliver different results. Therefore it is difficult to say what is happening here. This might have to do with the varying pressure ratios of the compressor for different RPM's, or that the NTC is placed in a location where the data is not very reliable. More research into the exact temperatures of the discharge is therefore advised.

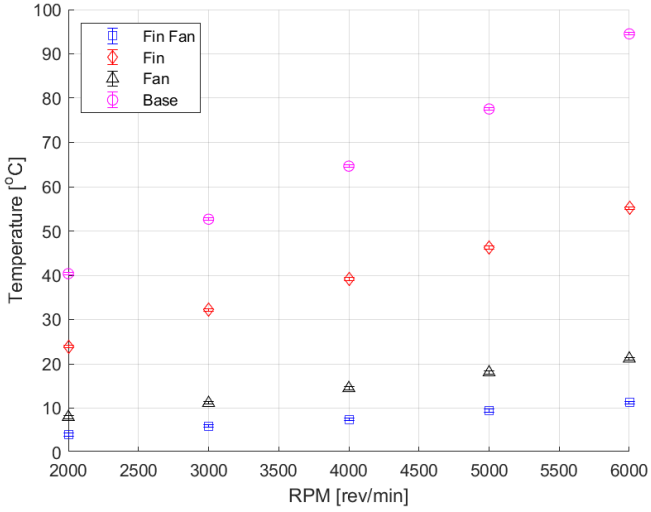

(a) 2 stage

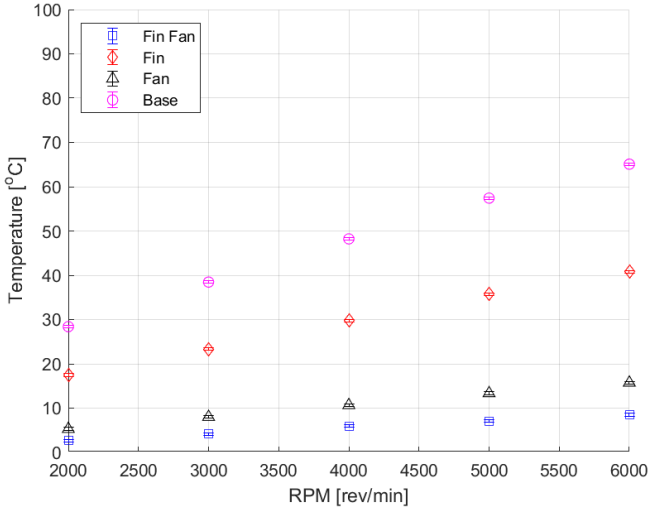

(b) 3 stage

Figure 4.13: Temperature difference between the wall of the compressor and the ambient air for different cooling settings per RPM. Here it is visible that because of the better heat transfer at the surface of the compressor the temperature difference is lower for the cooling settings that work better.

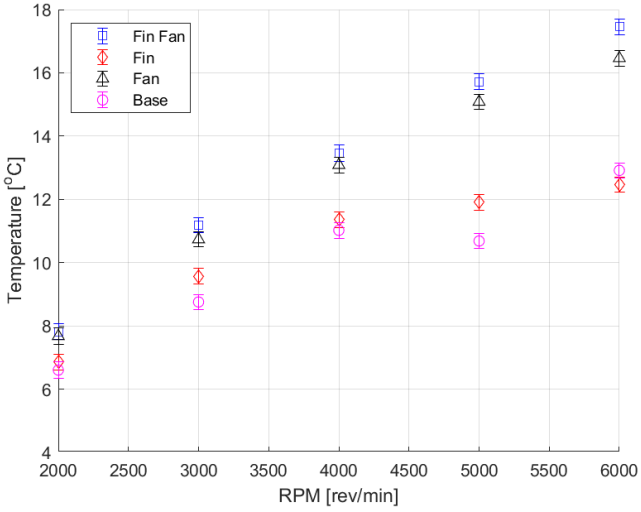

(a) 2 stage

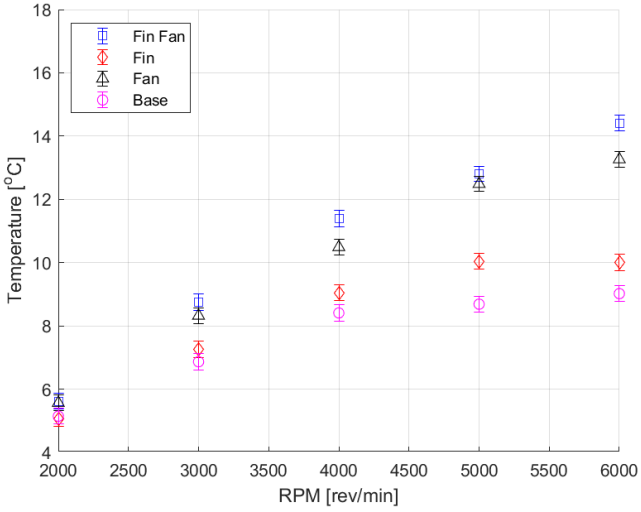

(b) 3 stage

Figure 4.14: Temperature difference between the wall of the compressor and the middle of the steel compressor housing for different cooling settings per RPM. Here the cooling settings that preform worse have a lower temperature difference. This is most likely due to the lower power consumption which is caused by the higher oil temperature as is visible in figure 4.17.

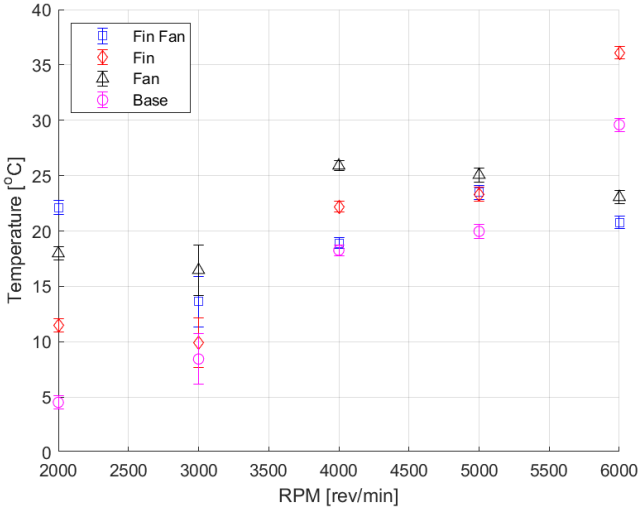

(a) 2 stage

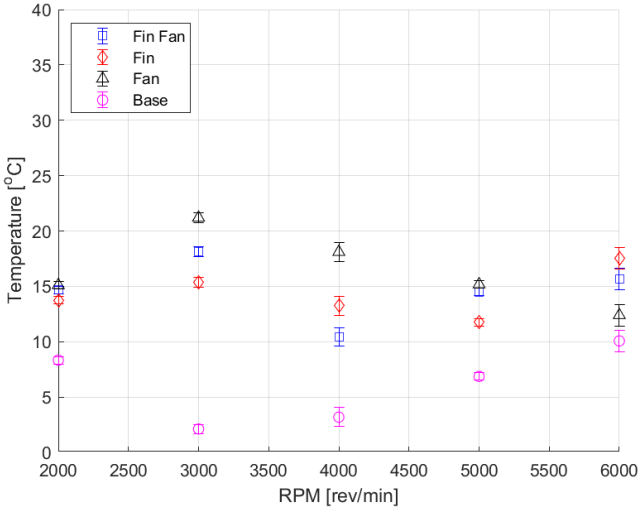

(b) 3 stage

Figure 4.15: Temperature difference between the fluid in the compression chamber of the compressor and the middle of the steel compressor housing for different cooling settings per RPM. Due to the randomness of the data no conclusions can be drawn from these figures. The only recommendation is to investigate the discharge temperature better.

4.3. TEMPERATURE DEPENDENCE

To asses the influence of the oil temperature on the mass flow and power usage of the system, the mass flow and power usages for the base cooling setting were calculated while the compressor was heating up to steady state. This was also done with the fin cooling setting. These two were chosen because they reached the highest temperatures over a longer period of time, making it possible to acquire more data.

4.3.1. MASS FLOW

For the mass flow of the compressor for different oil temperatures, the values were very scattered and no conclusion could be drawn from the figures as can be seen in figure 4.16. This would mean that the temperature of the oil does not have much influence on the mass flow of the compressor at the first stage of the system. However, from some initial testing of the higher stages there was a very distinct dependence on the mass flow of the system. These tests were however not done by the author of this thesis and the experimentation done was not extensive enough to include into this thesis. It is however strongly advised to do the temperature dependence experiments again for the higher stages of the system.

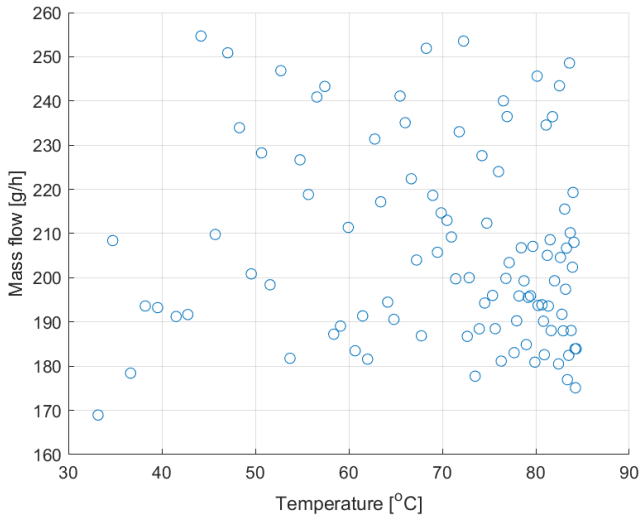

Figure 4.16: Mass flow at different oil reservoir temperatures. (at 3000 RPM, 2-stage, Base). The data is very scattered and therefore the conclusion can be made that for the first stage of the compressor, the temperature does not influence the mass flow of the system.

4.3.2. POWER USAGE

The power usage for different oil temperatures are depicted in figure 4.17. From this figure it can be stated that the friction forces inside the compressor are most likely directly

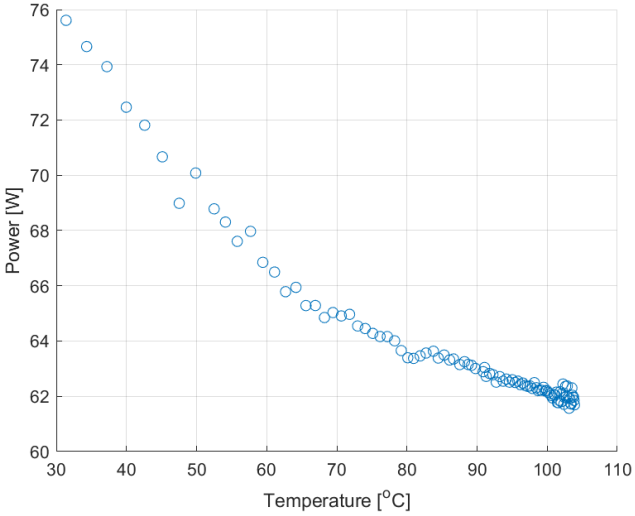

Figure 4.17: Power usage at different oil reservoir temperatures. (at 5000 RPM, 2-stage, Base). A clear correlation between the oil temperature and the power usage of the system is visible. This is likely due to the decrease in viscosity with higher temperatures which in turn reduces friction.

linked to the dynamic viscosity of the oil because the temperature vs dynamic viscosity curve typically follows a similar path. Because of this dependence it is interesting to find an oil with a certain viscosity at a certain temperature where the friction is decreased without decreasing the other performances of the compressor.

4.4. CARBON DIOXIDE MODEL

After verifying the model, it was used to asses the temperatures, mass flow and power usage of the entire system if the compressed gas were carbon dioxide instead of ambient air. The results will most likely differ from reality but might give a nice first estimation of the systems performance. For all the graphs presented in this section, the point at which the production reaches 336.7 [g/h] is marked with a red cross to indicate the performance of the system while it is in operation. The lines for the third stage of the 3 stage compression system are barely visible most of the time. That is because the third stage is not able to reach the pressure of 50 [bar] needed to open the valve of the compression chamber. This is most likely because the pressure difference between the compression chamber and the suction chamber is increased and the volume of the chambers is decreased a lot, while the measurement of the leakage paths are not changed. This resulted in a very high leakage for the higher stages.

4.4.1. TEMPERATURES

In figure 4.18 the discharge temperatures for the CO_2 compression system are shown. When looking at the figures it can be stated that the compressed gas would probably not reach temperatures exceeding the threshold of 100 [°C]. This is backed up by the fact that the model was overestimating the discharge temperatures for air. Therefore it can be stated that the compressor temperature would stay well below it's threshold for both the 2 and 3 stage systems.

4.4.2. MASS FLOW

The mass flows for the compression systems are depicted in figure 4.19. When comparing these values with the values gained from the model in figure 4.4, it is clear that the system with CO_2 is reaching the desired mass flow of 336.7 [g/h] at lower RPM's than when the system is modelled with air. It is therefore worth it to check whether the compressor might be able to reach it's target when operating with CO_2. The 3 stage system works very well for its first two stages. But as mentioned before, the third stage is not able to reach the target pressure of the outlet. This is why there is no production. How much mass flow can be induced when operating with CO_2 is again something that is not known, especially with regard to the higher stages.

From figure 4.20 it can be concluded that even though the 2 stage system works, it has a low volumetric efficiency for the first stage and an even lower volumetric efficiency for the second stage. This is again due to the scaling of the compressor volume and the increase of the pressure difference resulting in bigger leakages. While the 3 stage system starts of with a better volumetric efficiency, the thirds stage cannot produce any mass flow and is therefor 0% efficient.

4.4.3. POWER USAGE

The power usage of the CO_2 compression system for the 2 and 3 stage system is shown in figure 4.21. When comparing the 2 figures it seems that if you can get the third stage of the 3 stage system to work, the 3 stage compression train might run more efficiently than the 2 stage system. However, when looking at the differences between the model and the experimental values in figure 4.8, it is visible that the friction losses were underestimated with about a factor 5x. This means that the friction forces are probably more dominant than modelled. This might result in much more friction losses for the 3 stage system because it would require 3 stages to run instead of 2. However, this is only an estimation and the compression systems would first need to be tested with CO_2 before definite conclusions can be formed.

Finally, using the calculated power usage and mass flow, the compressor efficiencies can again be calculated which are depicted in figure 4.22. When comparing these results with the results shown in figure 4.7, the assumption can be made that the compressor efficiency will probably lay a lot lower at around 15-20% instead of 40-50%.

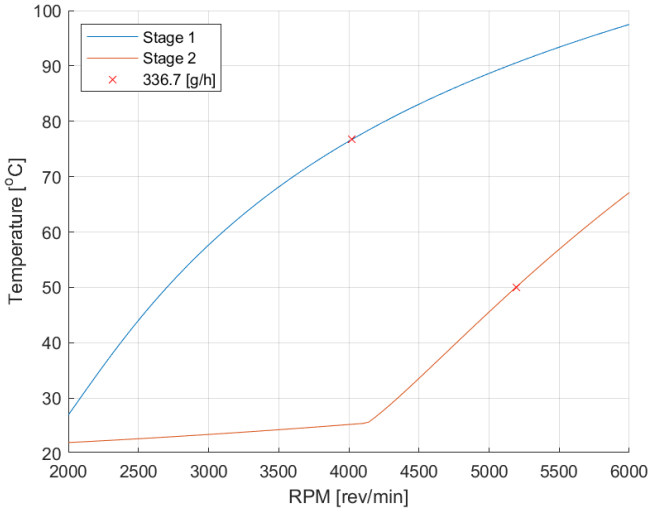

(a) 2 stage

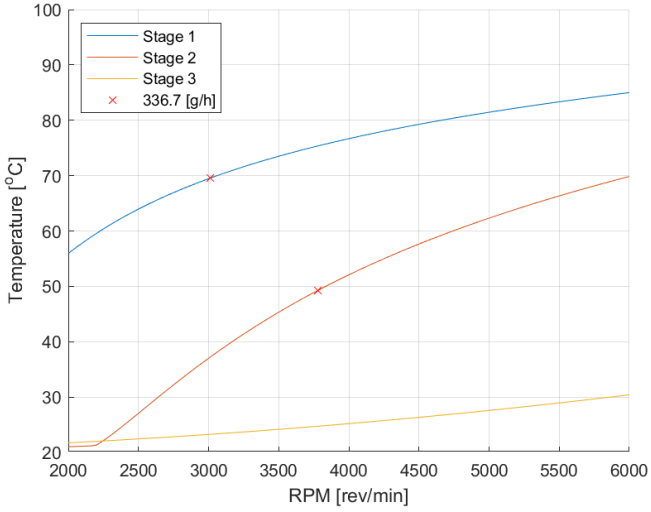

(b) 3 stage

Figure 4.18: The maximum temperature of the carbon dioxide inside the compressor. The modelled temperature stays below the temperature threshold. However the third stage is not able to produce a mass flow and therefore has a very low temperature.

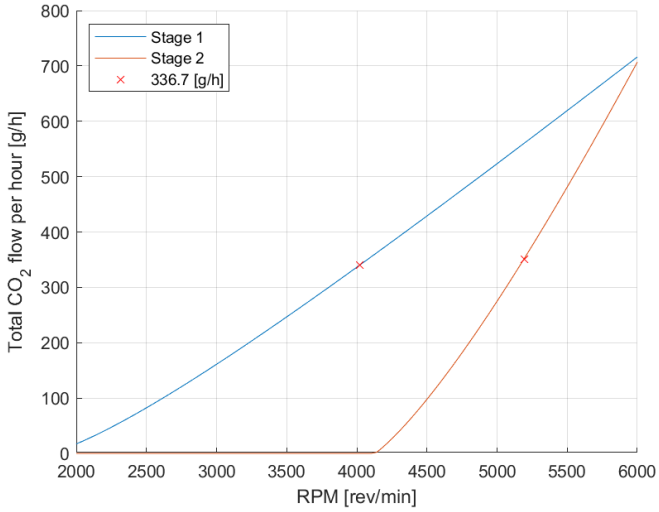

(a) 2 stage

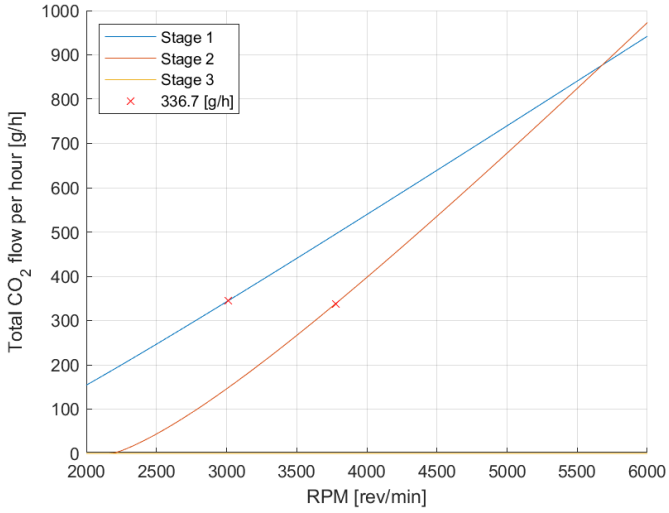

(b) 3 stage

Figure 4.19: The mass flow of the carbon dioxide induced by the compressor. The mass flow for CO_2 is higher than the model predicted the mass flow using air as the compressed medium. This can be seen by comparing the figures with figure 4.4. The third stage of the 3 stage system is not producing mass flow because the desired pressure could not be reached in the compression chamber.

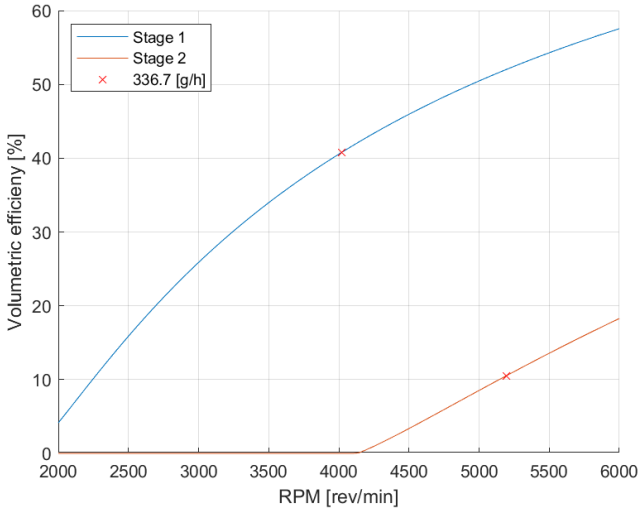

(a) 2 stage

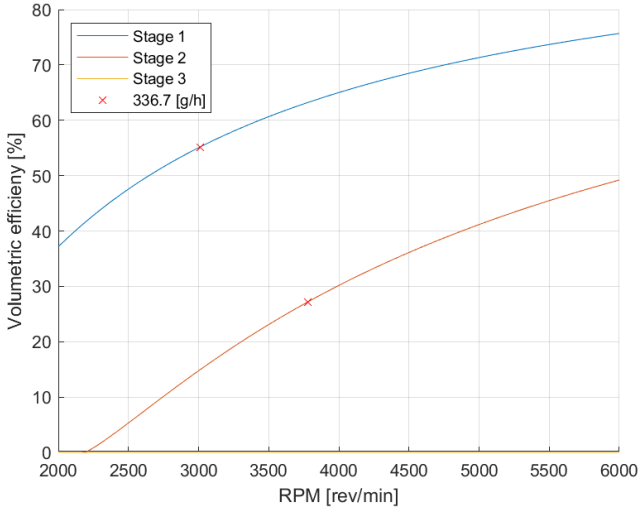

(b) 3 stage

Figure 4.20: The volumetric efficiency of the compressor when compressing CO_2. The volumetric efficiencies are low for the 2 stage system and higher for the 3 stage system with an exception for the third stage.

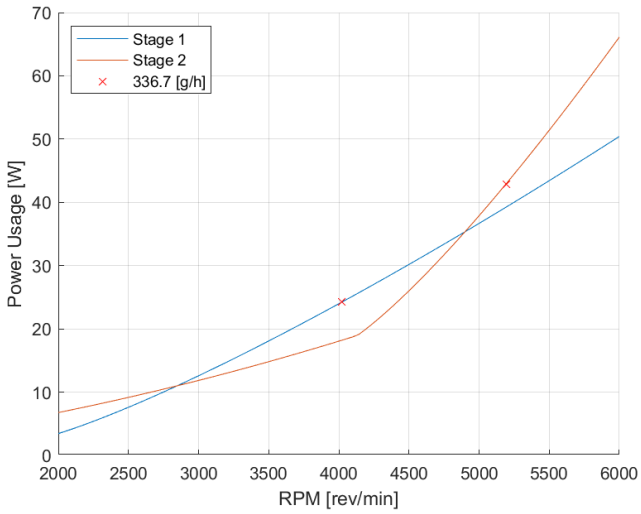

(a) 2 stage

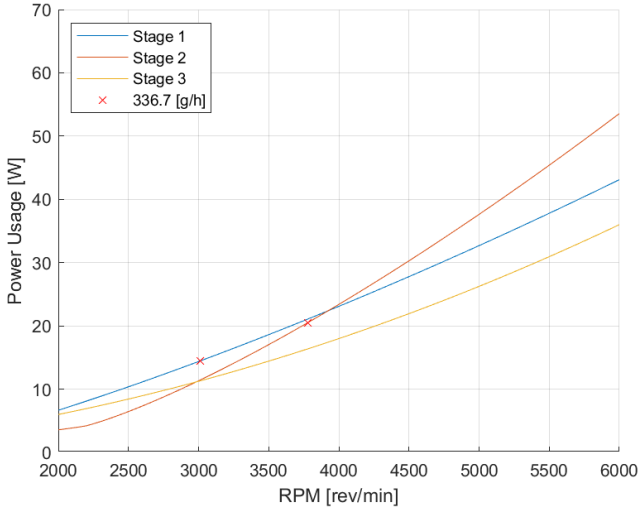

(b) 3 stage

Figure 4.21: The power usage of the compressor needed to compress the carbon dioxide. The total power usage of the 2 stage system seems to be higher, however this is hard to validate because the point at which the third stage of the 3 stage system would operate is non existing. And because of the underestimation of the friction losses inside the system, the 3 stage system would most likely preform even worse.

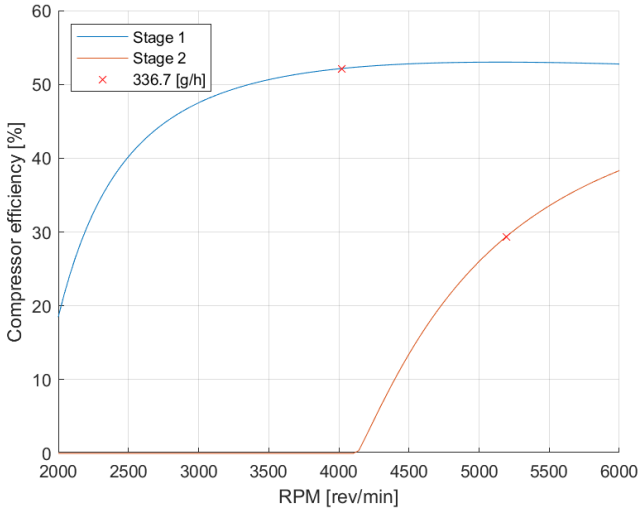

(a) 2 stage

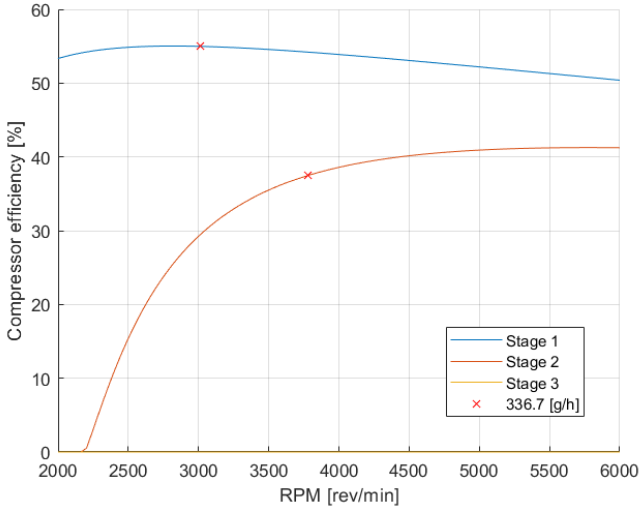

(b) 3 stage

Figure 4.22: The compressor efficiency when compressing CO_2 for the 2 and 3 stage system. The 3 stage system is again more efficient for the earlier stages but losses ground due to the third stage does not work.

5

CONCLUSIONS

This work was conducted to get a better understanding what the relevant phenomena are when CO_2 is compressed for low mass flows using rolling piston compressors, and what the ideal amount of stages is. This chapter will elaborate the conclusions that were drawn from the work done on the computational model and the experimentation. Afterwards, the research questions proposed in chapter 1.2 are answered.

5.1. COMPUTATIONAL MODEL

Most of the calculations done by the computational model seemed to be off by quite a margin. However, that was to be expected because no research had been done into this subject before the start of this thesis.

Steady state temperatures First of all, the heat transfer through the compressor casing was either overestimated or underestimated for certain sections, with the exception of the air to casing wall section. The under and overestimation was most likely due to the oversimplification of the system. Eventually, the experimentation did however show that the discharge temperatures inside the compressor were lower then the modelled values. This was a positive deviation, since a lower discharge temperature was preferable.

Mass flow The mass flow was estimated more accurately, but still seemed to differ at higher and lower RPM's, which was most likely due to the different operating pressures caused by the solenoid valve and the pressure drop created by the check valve. The 2 stage system did not seem to reach the desired mass flow. That might be improved by fixing the way the mass flow is measured, but research into the scaling of the compression chambers together with the influence of oil flow is advised.

Power Usage The power usage of the system seemed to be underestimated by the model. This was mostly due to the underestimation of the frictional losses of the compressor.

The experimentation done on the cooling power of the compressor was not very reliable but was not detrimental for the research goals of the thesis.

5.2. ACTIVE COOLING

The active cooling settings assessed in chapter 4.2 seemed to show that only 3 compressor settings could keep the compressor cool enough, being:

- a 2 stage cooled system with fins and a fan.
- a 3 stage cooled system with fins and a fan.
- a 3 stage cooled system with only a fan.

From chapter 4.3 it also became clear that at least for the first stage of the compression train, it is interesting to either keep the compressor running hotter or to decrease the viscosity of the lubrication to reduce the impact of friction on the system.

Therefore it can be stated that the number of stages needed for the compression system regarding the temperature inside the compressor can be reduced from 4 stage as mentioned in chapter 2.2.1 to a 2 stage system with the use of active cooling. This finding is very beneficial because by reducing the amount of stages, the internal leakages and friction losses of the compression system can be reduced. Thereby increasing the effectiveness of the system.

5.3. OPTIMAL AMOUNT OF STAGES

The main goal of this thesis was to asses what would be the optimal amount of stages for the compression system needed to compress CO_2 with the constraints set in chapter 1.1.3. This thesis was focused on the double and triple stage system, to see which system outperforms the other and to see if active cooling could reduce the amount of stages needed for the system. In table 5.1, each stage is ranked and each ranking is explained in the following paragraphs.

# of Stages	Temperature	Mass Flow	Power Usage	Initial Cost
2	+	+	-	+
3	++	- -	-	-

Table 5.1: Each system ranked in the four most relevant categories to asses which system performs better.

Temperature The temperature inside the compressor is very important because it determines how long the lubrication can last. The 3 stage system was able to keep the compressor very cool and therefore gets a maximum score of (++). The 2 stage system seemed to become somewhat hotter but was still capable of staying below the threshold. Therefore it gets a slightly lower but still good score of (+).

Mass flow The mass flow of the system is important to ensure the right molar balance in the methanol reactor after the compression stages. The 2 stage systems scores well because even though the first stage of the system seemed to perform worse then 3 stage system, the 3 stage system was not able to achieve the needed pressure at the final stage; thereby producing no mass flow. Therefore, the 3 stage system received the lowest score of (- -) while the 2 stage system received a decent score of (+).

Power usage The power usage is important because the ideal system should be as efficient as possible to improve the overall efficiency of the micro plant. The power usage seemed to be somewhat similar for both systems and they both were not very efficient. Therefore they both received a score of (-).

Initial cost One of the main advantages of running a 2 stage system instead of a 3 stage system is that the initial cost can be lowered, because one less compressor is needed. Therefore the 2 stage system receives a (+) while the 3 stage system receives a (-). Reducing costs is not only beneficial for companies that work with these compressors but can also ensure cheaper prices for methanol production or other products that need compressed carbon dioxide in their manufacturing process.

Ideal system: 2 stage When looking at table 5.1 it is clear that the 2 stage system outperforms the 3 stage system. Only the temperature regulation of the 3 stage system seems to work better. However, because the temperature regulation of the 2 stage system is also decent, the 2 stage system is still the better pick for a compression system for high pressures and low mass flows using rolling piston compressors.

Validity The validity of the statement of the ideal system is however not undeniable since not enough experimentation has been done on the higher stages of the system and because the computational model seemed to still differ a lot from the values extracted from experimentation. Therefore multiple recommendations can be done regarding the research topic of this thesis, which will be done in chapter 6.

6

RECOMMENDATIONS

The recommendations are split up into two parts. First, the computational recommendations are discussed in section 6.1. Second, the experimental recommendations are discussed in section 6.2.

6.1. CHANGES IN COMPUTATIONAL MODEL

Pressure calculation The pressure calculations can be improved further. At first, the assumption of constant specific heat was made because air was used in the system. For CO_2, the assumption is not valid and therefore the pressure increase will have to be calculated differently. It might be possible to model the pressure increase using the database from [NIST Standard Reference Database, 2010].

Secondly, the effects of oil flow on the dead volume and energy balance of the system are not taken into account in this model. It is strongly advised to do more research on the impact of these oil flows.

Finally, The leakage rate calculations were a very rough estimation and only the radial leakages were taken into account. For the follow-up research, it is advised to improve the leakage rate calculations and also calculate the leakages for the other leakage paths.

Heat transfer From the experimentation, it was clear that the assumption of no 3D heat transfer was not valid. Therefore it is advised to rewrite the heat transfer model into a 3D model with heat exchange to the oil around and the gas above the compressor.

Also, the heat transfer out of the compressed fluid was clearly underestimated because the discharge temperatures of the experimentation were a lot lower than the values the model calculated. It is interesting to investigate whether the heat transfer is higher for the compressing fluid or that the atomization of the lubricant is actually occurring inside the compressor resulting in a lower discharge temperature.

Losses and Optimization The calculation of the friction losses were not accurate. Therefore these calculations need to be remodelled to better calculate these losses.

If at some point, a model is created that can more accurately describe the functionality of the compressor, it might be interesting to do an optimization study on the compression system to improve the performance of the compressor.

6.2. CHANGES IN EXPERIMENTAL METHOD

Inlet Conditions The experimentation for this thesis was done with ambient air because high concentrations of CO_2 in the air can be hazardous to humans, because it can deprive them of oxygen. However to better understand the differences between air and CO_2 it is best to do experimentation with CO_2 in a fume hood.

During the experimentation of the compressor, some of the water which was present in the ambient air seemed to condense after compression. This causes rusting of the internal components and might decrease the validity of the results. Therefore it is advised to ensure the inlet of the compression train has at most 2% water saturation, to ensure the water does not condense after compression.

Instrumentation The instrumentation used to measure and regulate the experimentation did not always gain the desired results. From the experimentation performed for this thesis, it became clear that the discharge temperature was not very reliable. Therefore it is advised to conduct more experiments using different methods to asses the discharge temperature.

The pressure regulation of the compressor was not constant for all tested RPM's. Because of this difference, the pressure difference and pressure ratio's differ for each RPM. This in turn reduces the validity of the mass flow experiments. Therefore it is advised to change the pressure regulation of the system to yield more consistent results for different RPM's. Also, a different check valve with a lower pressure drop might prove useful to make the results of the experiments better. Finally, the pressure regulation might be fixed easily by increasing the pressure vessel volume.

The results for the cooling power of the experimentation were most likely not precise, nor accurate. To improve the results, more research needs to be done into the exact flow generated by the fan, and the temperature sensors would need to be more more precise and accurate for the range in which they are operating.

Higher Stages For this thesis only the first stage of each compression train was experimented on, because most of the research was focused on the thermodynamics of the system and not on the mass flow. But to truly validate the model, it is recommended that the higher stages are also experimented on.

A

EQUIPMENT CALIBRATION

For the repeatability of all the experiments that were conducted, the measuring devices (appendix A.1) and measuring inaccuracies (appendix A.2) are elaborated in this appendix.

A.1. MEASURING DEVICES

In this section, the measuring devices that were used are explained together with the standard deviations of the devices.

A.1.1. TEMPERATURE SENSORS

To measure the temperatures in and around the compressor, negative temperature coefficiencts (NTC's) were used. The NTC's used were 100 [kΩ] at 20 [^{o}C]. To measure the temperatures at around 60 to 80 [^{o}C] more accurately, a 8.2 [kΩ] resistance was used in series with the NTC's. Once all the NTC's were installed, the average temperature over all NTC's was calculated together with the standard deviation. The standard deviation was set to the same value for all the NTC's, except for the NTC's that were measuring the inlet and outlet of the air of the fan duct. This was done because the compressor seemed to have a different temperature then the ambient air. The standard deviation of compressor NTC's was calculated to be 0.151 [K] and the air NTC's were 0.124 [K].

A.1.2. PRESSURE SENSOR

The pressure sensor that was used was a sensor that measured the pressure difference with the ambient pressure. This sensor had a range from -1 to 9 [bar], meaning that it would probably measure the pressures of the lower stages quite accurately. For this sensor, no standard deviation measurements were made because at the time there was no sensor to accurately calculate the standard deviations. However, because the sensor had been used on different experimentation before in which it was rigged the same way, the decision was made that no further testing was needed.

A.1.3. CURRENT SENSOR

For the current measurement of the DC current going to the electrical board of the compressor, an ACS712 20A was used because the maximum current that the compressor can draw before shutting down is 20 [A]. To measure the standard deviation of the sensor, the compressor was turned on at different rotational speeds and was then measured with the ACS712 and an external current sensor at the same time. The values from both current sensors were much alike and after extensive testing, the standard deviation was determined to be 0.005 [A]. The power usage of the electrical board was very hard to determine once the compressor was turned on. However, when the compressor was not running the current usage of the board could easily be calculated; which was 0.03 [A].

A.1.4. WATER SEAL AND FAN

The water seal that was used to determine the pressure drop was tested for 2 possible setups: with and without fins. From this experimentation, there seemed to be no difference between the 2 setups since they both showed a water level difference of 4 [mm], which corresponds to a volumetric flow rate of 0.0743 [m^3/s] according to figure 3.8. This is however a very rough estimate because it was not possible to measure the pressure drop more accurately. Luckily, this proved to be not very important for measuring the cooling power, because the inaccuracy of the temperature sensors when assessing the cooling power was a lot more influential.

A.2. MEASURING INACCURACIES

During the experimentation, some inaccuracies of the system were discovered. These inaccuracies are further explained in this section.

A.2.1. SOLENOID VALVE

The chosen method for the automatic pressure regulation was to release the pressure of the vessel by shortly opening a solenoid valve. The solenoid valve was set to open for 150 [ms] in the 2 stage system and 335 [ms] for the 3 stage system. This was done so the compressor would be able to regulate the pressure at maximum RPM. After some time experimenting, it became clear that the maximum and minimum pressures of the system before and after the opening of the solenoid valve was different for both systems, which is visible in figures A.1 & A.2.

From these figures, it is clear that the there is a big difference between the compressor experiments at lower and higher RPM's. Sadly, the deviation of maximum and minimum pressures was discovered late in the experimentation process. Therefore, the decision was made to finish the experimentation with the current set-up. However, the deviation might have a high impact on the performance of the system and the validity of the results. Therefore, recommendations were made to change the way the pressure is regulated for further experimentation in chapter 6.2.

A.2.2. CHECK VALVE

After the experimentation was completed, the check valve was evaluated because check valves usually cause a pressure drop. This was tested and the check valve that was used

	No Check Valve		Check Valve	
Total # Stages	2	3	2	3
Pressure Difference [bar]	2.7	6.1	2.8	6.2
Pressure Ratio	3.7	7.1	4.2	8.0

Table A.1: The difference between the pressure difference and pressure ratio over the compressor with and without the check valve installed.

seemed to have a pressure drop of 0.111 [bar]. A pressure drop of this size would disrupt desired pressure ratio and pressure difference induced by the compressor, as is visible in table A.1.

While the pressure difference is not affected that much, the pressure ratio does change a lot. Therefore the temperature increase due to compression might actually be higher in the experimentation than it should have been.

A.2.3. VESSEL LEAKAGE

While the pressure vessel was under pressure, the vessel was not perfectly sealed off and had some leakage. The leakage rate at 3.7 and 7.1 bar could however be calculated by closing all the valves and measuring the pressure drop over time. The leakages were between 0.5 and 0.7 [mg/h], which is very low when compared to the desired compressor mass flow of 336.7 [g/h]. Therefore the leakages were not taken into account for the mass flow calculations.

A

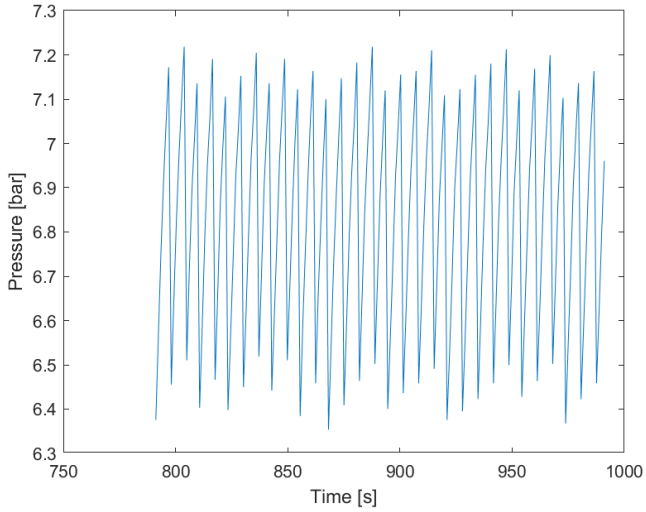

(a) 2000 [RPM]

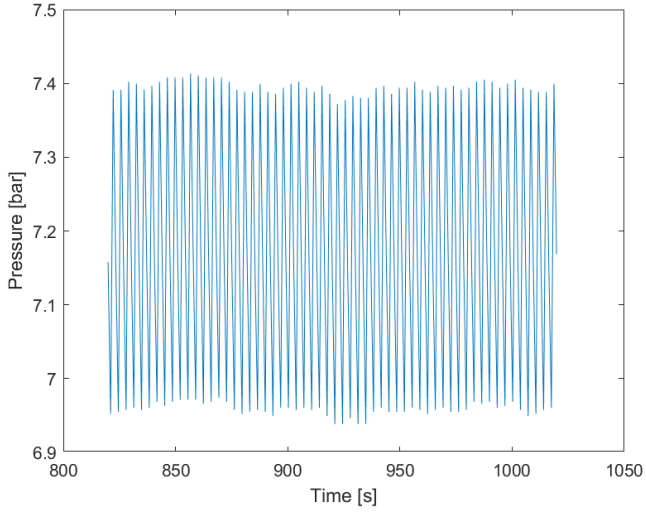

(b) 6000 [RPM]

Figure A.1: The pressure inside the vessel over the last 200 seconds of the steady state experiments for the first compressor of the 2 stage system. When comparing the 2 graphs it is visible that the pressure regulation has different maxima and minima for different RPM's.

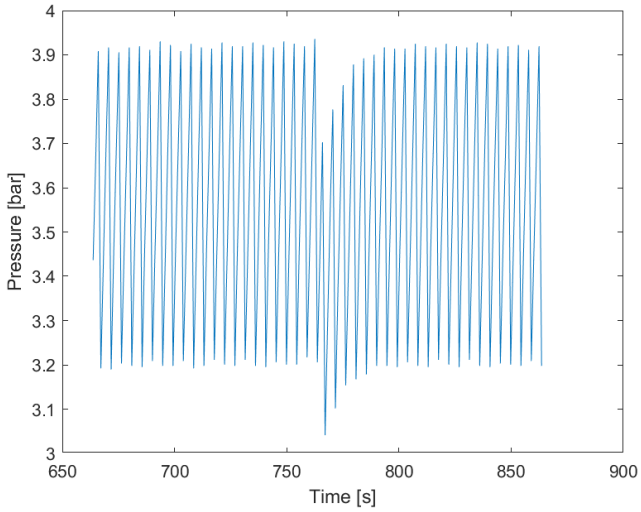

(a) 2000 [RPM]

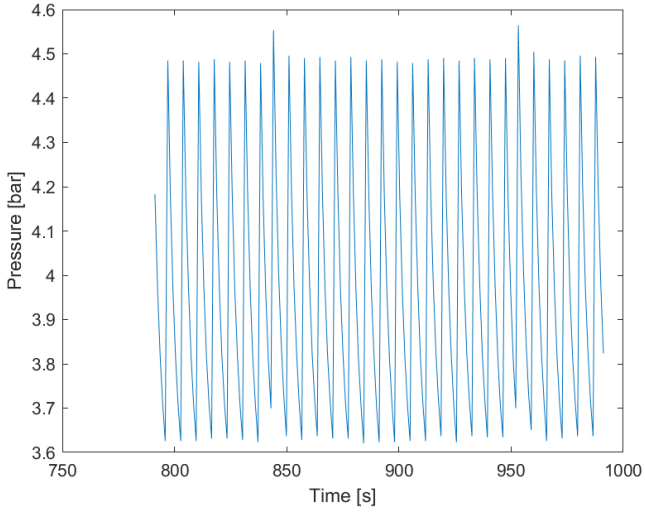

(b) 6000 [RPM]

Figure A.2: The pressure inside the vessel over the last 200 seconds of the steady state experiments for the first compressor of the 3 stage system. When comparing the 2 graphs it is visible that the pressure regulation has different maxima and minima for different RPM's

BIBLIOGRAPHY

Bergstein, P. (2020). *Development of a high pressure,low flow rate carbon dioxide compressor*.

Boukais, B., & Zeroug, H. (2004). Efficency determination of a brushless dc motor under field weakening operation. *Progress in Electromagnetic Research Symposium*, 567–570.

Bruno, T. J., Bruno, T. J., Fortin, T. J., Huber, M. L., Laesecke, A., Lemmon, E. W., Mansfield, E., McLinden, M. O., Outcalt, S. L., Perkins, R. A., et al. (2019). *Thermophysical properties of polyol ester lubricants*. US Department of Commerce, National Institute of Standards; Technology.

de Koning, R. (2020). *Research and design of a co2 compressor for implementation in a methanol micro-plant*.

Dwyer, T. (2020). Module 163: Rolling-piston rotary refrigerant compressors for air conditioning applications. https://www.cibsejournal.com/cpd/modules/2020-06-toshiba/

Engineering ToolBox. (2003). Hydraulic diameter [Online; accessed 22-4-2021]. https://www.engineeringtoolbox.com/hydraulic-equivalent-diameter-d_458.html

Goswami, D., Shah, D., Jotshi, C., Bhagwat, S., Leung, M., & Gregory, A. (1997). *Foaming characteristics of refigerant/lubricant mixtures* (tech. rep.). Florida Univ., Gainesville, FL (United States).

Grützner, T., Ziegenbalg, D., & Güttel, R. (2018). Process intensification–an unbroken trend in chemical engineering. *Chemie Ingenieur Technik*, *90*(11), 1823–1831.

Guanyu Tube. (2021). Fin Tube Heat Exchanger Manufacturing Process Classification [Online; accessed 22-4-2021]. https://tubingchina.com/fin-tube-heat-exchanger-manufacturing-process-classification.htm

GYZS. (2021). Roval Aluminium u-profiel 15 x 15 x 15 x 2mm [Online; accessed 22-4-2021]. https://www.gyzs.nl/roval-aluminium-u-profiel-15-x-15-x-15-x-2mm.html?dfw_tracker=93579-1460425&gclid=Cj0KCQjwvYSEBhDjARIsAJMn0lia5%20YzU3ykPyZOrFyb-GxhB0-LjP768FuuCThmAJaoAYFJZGJUfEsEaAgW7EALw_wcB

Hardy, J. T. (2003). *Climate change: Causes, effects, and solutions*. John Wiley & Sons.

Ikeuchi Europe. (2019). Classification of spray droplet diameter [Online; accessed 14-01-2021]. https://www.ikeuchi.eu/news/measurement-of-droplet-size/

Kim, G.-w., Noh, K.-y., Min, B.-c., Song, S.-j., Na, S.-k., Yoon, T.-s., Teshima, K., Yang, J.-s., Choi, G.-m., & Kim, D.-j. (2016). Prediction of leakage flow of radial clearance in a rolling piston rotary compressor.

Kremer, R., Barbosa Jr, J. R., & Deschamps, C. J. (2012). Cooling of a reciprocating compressor through oil atomization in the cylinder. *HVAC&R Research*, *18*(3), 481–499.

Kremer, R., Deschamps, C. J., & Barbosa, J. R. (2008). Theoretical analysis of the effect of oil atomization in the cylinder of a reciprocating ammonia compressor.

Majithia, A., Hall, S., Harper, L., & Bowen, P. (2008). Droplet breakup quantification and processes in constant and pulsed air flows. *Proceedings of the 22nd Conference on Liquid Atomization and Spray Systems (ILASS-Europe), Como Lake, Italy*, 8–10.

Mills, A. (2014). *Basic heat and mass transfer* (second). Pearson.

Moran, M., Shapiro, H., Boettner, D., & Bailey, M. (2012). *Principles of engineering thermodynamics* (seventh). Wiley.

Ningbo Longxuan Aluminium Co., Ltd. (2021). Competitive price trustworthy cylindrical heat sink [[Online; accessed 22-4-2021]]. https://www.alibaba.com/product-detail/Competitive-price-trustworthy-cylindrical-heat-sink_60460093554.html

NIST Standard Reference Database. (2010). *Nist reference fluid properties* (Version 9.0). https://www.nist.gov/srd/refprop

Ooi, K. (2005). Design optimization of a rolling piston compressor for refrigerators. *Applied thermal engineering, 25*(5-6), 813–829.

Padhy, S. (1994). Lubrication analysis of a rolling piston rotary compressor: Part 1: Mathematical modelling. *Proceedings of the Institution of Mechanical Engineers, Part J: Journal of Engineering Tribology, 208*(2), 83–94.

Pandeya, P., & Soedel, W. (1978). Rolling piston type rotary compressors with special attention to friction and leakage.

Parker. (2012). *Chemicals, lubricants and accessories. catalog g-1* (tech. rep.). Parker Hannifin Corporation. https://www.parker.com/Literature/Sporlan/Sporlan%5C%20pdf%5C%20files/Sporlan%5C%20pdf%5C%20Miscellanous/Catalog%5C%20G-1%5C%20Chem%5C,%5C%20Lubricants%5C%20and%5C%20Acc.pdf?elqTrackId%5C=56abcc593f9e43018b09e8328cba6b97%5C&elqaid%5C=10333&elqat%5C=2

Ratzlaff, J. (2018). Hydraulic diameter of a regtangular tube [Online; accessed 22-4-2021]. https://www.piping-designer.com/index.php/properties/fluid-mechanics/2254-hydraulic-diameter-of-a-rectangular-tube#:~:text=The%5C%20hydraulic%5C%20diameter%5C%2C%5C%20abbreviated%5C%20as,the%5C%20diameter%5C%20of%5C%20the%5C%20shape.

Sinnott, R., & Towler, G. (2013). Chapter 19 - heat-transfer equipment. In G. Towler & R. Sinnott (Eds.), *Chemical engineering design (second edition)* (Second Edition, pp. 1047–1205). Butterworth-Heinemann. https://doi.org/https://doi.org/10.1016/B978-0-08-096659-5.00019-5

Subiantoro, A., & Ooi, K. T. (2019). Dynamic characteristics of rolling piston machines. *Positive displacement machines* (pp. 263–289). Elsevier.

Tachibana, F., & Fukui, S. (1964). Convective heat transfer of the rotational and axial flow between two concentric cylinders. *Bulletin of JSME, 7*(26), 385–391.

Thermopedia. (2011). Comparison of fully developed temperature profiles in two plates cooled by the same fluid [Online; accessed 14-01-2021]. http://www.thermopedia.com/content/585/

Yanagisawa, T., Shimizu, T., Chu, I., & Ishijima, K. (1982). Motion analysis of rolling piston in rotary compressor.